Chapter 6

SOLITON INSTABILITY

A covert answer to his seeking came
In a far-shimmering background of Mind-space..
Sri Aurobindo in Savitri, -p 289

6.1 Introduction

In this chapter we address ourselves to nonlinear optical effects on non-singular topological defects called kinks or walls. We have already described briefly in chapter 1 the director distortions associated with these defects [1, 2]. As remarked earlier these are unlike true solitons and they do not preserve their shape and velocity after a pairwise collision. Their structures have been well studied in various situations. Yet these kink structures have not attracted much attention of the workers in nonlinear optics.

We have already seen that the electric field associated with a laser beam is known to simulate the effect of an external static electric or magnetic field since the free-energy density of the nematic depends quadratically on the field. The coupling between the director and the electric field of the laser beam arises due to optical dielectric anisotropy. In such cases it is neccessary to solve self-consistently both the equations of elastic equilibrium and Maxwell equations of electrodynamics. We have worked out in this chapter the structural transitions between different permitted kinks in the presence of a laser field and a static magnetic field. We consider only nematics and a nematic doped with ferromagnetic grains in the following.

6.2 Kink States in a Nematic

In a nematic, with positive diamagnetic anisotropy, n can be either parallel or antiparallel to the external field [3]. When the director in one state which is parallel

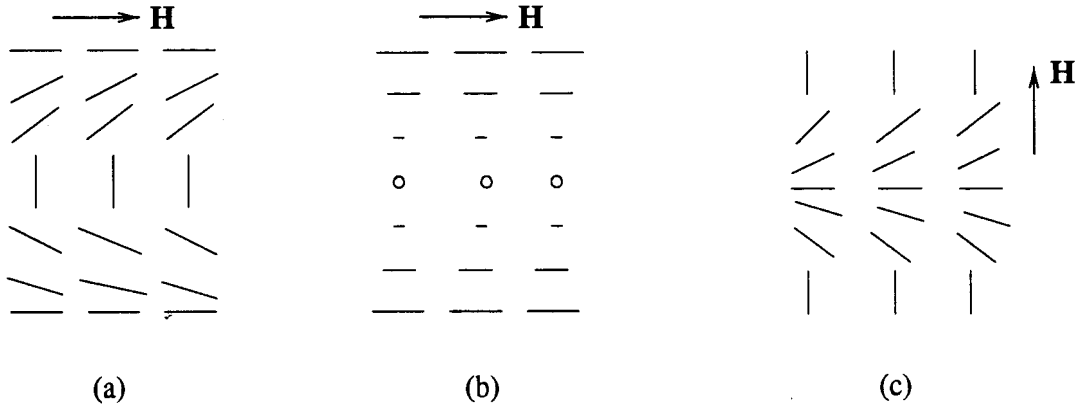

Figure 6.1: *The director configuration in (a) a bend-rich wall, (b) a twist wall and (c) a splay-rich wall in an external magnetic field H.*

to the field H is connected to the director in the other state which is antiparalel to the field, we get a *'wall'* or a *'kink'*. There could be three types of walls in nematics depending on the nature of the associated director distortions. They are the *bend – rich* wall, the *twist* wall or *splay – rich* wall. In a bend-rich wall the director is restricted to a plane and the director turns through 180° from one end to another. Its structure is shown in the figure 6.1 (a). In the case of a twist wall the director rotates through 180° perpendicular to H. Its structure is shown in figure 6.1 (b). The director configuration in a splay-rich wall is depicted in figure 6.1 (c). It is easy to see that a bend-rich wall has not only bend distortions but also splay distortions in it but is dominated by bend distortions. Hence, we prefer to call the bend wall a 'bend-rich' wall. Similarly, a 'splay-rich' wall is dominated by splay distortions.

We can get similar kinks or walls even in the presence of an optical field of a laser beam [4]. We start with the free-energy density of a nematic which has contributions from both the elastic deformations and externally applied fields. In the one elastic constant approximation and with a static magnetic field the free-energy

density is given by the sum of free-energy densities

$$\mathcal{F}_{elastic} = \frac{K}{2}\left[(\nabla \cdot \mathbf{n})^2 + (\nabla \times \mathbf{n})^2\right] \tag{6.1}$$

and

$$F_{mag} = -\frac{\chi_\perp}{2}H^2 - \frac{\chi_a}{2}(\mathbf{n} \cdot \mathbf{H})^2 \tag{6.2}$$

In the absence of the laser beam, $\mathbf{n}$ will be either parallel or perpendicular to the magnetic field depending on whether χ_a is positive or negative.

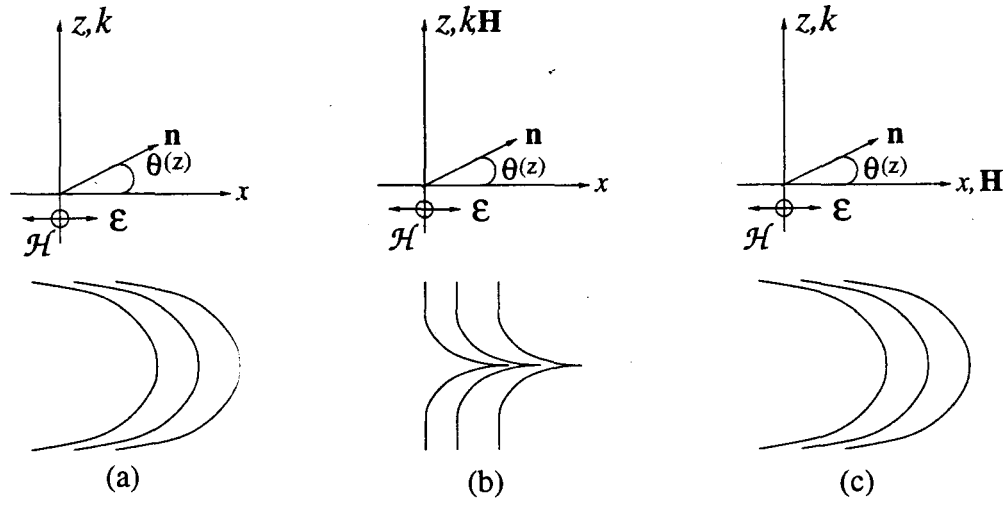

Figure 6.2: *Geometries showing the orientation of the director* $\mathbf{n}$ *with respect to the electric field* $\mathcal{E}$ *of the incident light and a static magnetic field H. (a)* $H = 0$*; (b) H is perpendicular to* $\mathcal{E}$*, and (c) H is parallel to* $\mathcal{E}$*. k is the direction of propagation of the light,* $\mathcal{H}$ *is the magnetic vector associated with the light which is perpendicular to the plane of the figure.*

In this chapter. we consider only a splay-rich or bend-rich kink state with its director confined to the x – z plane and having $\mathbf{n}$ varying along $\mathbf{z}$. Also we restrict ourselves to a linearly polarised light wave propagating along the z-axis with its electric vector $\mathcal{E}$ along the x-axis. Then field $\mathcal{E}$ variations are also along the z. The geometry is depicted in figure 6.2 (a). It is easy to see from the geometry of figure 6.2 (a) that the polarisation of the light wave is preserved during its passage through the splay-rich kink. The Maxwell wave equation is solved in the approximation that the director distortions in the medium are on a length scale large compared to the wavelength of light. Then as was shown in chapter 1, the optical field free

energy density is given by:

$$\mathcal{F}_{optical} = -I\frac{(\epsilon_{\|}\epsilon_{\perp})^{\frac{1}{2}}}{(\epsilon_{\perp} + \epsilon_a \sin^2\phi)^{\frac{1}{2}}} \tag{6.3}$$

where $\mathbf{I}(=\frac{|A|^2}{8\pi c}(\epsilon_{\|}\epsilon_{\perp})^{\frac{1}{2}})$ is a measure of the intensity of light. $\boldsymbol{A}$ is the amplitude of the light wave. It must be remarked that in the geometry shown in figure 6.2 (b) for a twist wall or a bend-rich wall the phase varies across the wavefront as it propagates through the kink structure. Hence we consider only splay-rich walls. Likewise, in geometry shown in figure 6.2 (c) we consider only bend-rich walls because in the other two cases the polarisation and or phase varies across the wavefront.

To make our point clear we discuss briefly the problem associated with a twist wall in the geometry shown in figure 6.2 (c), applicable to cases with director distortions along the direction of light propagation. The direction of light propagation is then along the twist axis. We work in the approximation that the director distortions are on a length scale very large compared to the wavelength of light. Then this leads to the Mauguin limit or adiabatic limit. In this limit as already said, the base states are linearly polarised parallel or perpendicular to the local director. Hence if the incident light is polarised parallel to the director, initially, then it remains always parallel to the local director. This does not result in any change in the director configuration as it does not lead to any optical torque on the director. Only at low magnetic fields this approximation is valid and the wall structure is unaffected. At higher magnetic fields this approximation breaks down since the wall thickness may become comparable to or less than the wavelength of light. In such cases we find that there could be reflection of light by the soliton and also the polarisation state of laser wave is not preserved as it propagates through the soliton. This situation is quite complex to analyse and a complete solution will be an involved numerical exercise of finding the solution of Maxwell's equations and the equations of elastic equilibrium.

In view of these difficulties we have confined our studies to the planar distortions involving splay-rich and bend-rich kinks only. The splay-rich and bend-rich kinks involve both type of distortions and no qualitative changes are found if elastic

anisotropy(splay elastic constant being not equal to the bend elastic constant) is included. In fact we observe that the elastic anisotropy leads only to an increase or a decrease in the thickness of the kink. Hence, to extract the salient features we work in the one constant approximation.

6.2.1 Kinks in an optical field

We first study kinks permitted in an optical field. The relevant geometry is that shown in figure 6.2 (a). The total free-energy density for planar distortions is [5, 6]:

$$\mathcal{F} = \frac{K}{2}\left(\frac{\partial\phi}{\partial z}\right)^2 - \frac{I\,\epsilon_{\|}^{\frac{1}{2}}}{(1 + \tau\,\sin^2\phi)^{\frac{1}{2}}} \tag{6.4}$$

Here $\tau = \epsilon_a/\epsilon_\perp$. The kink state has only splay-bend distortions in the director (see figure 6.1 (a)). Minimisation of the total free energy leads to

$$K\frac{\partial^2\phi}{\partial z^2} = \frac{\mathbf{I}\,\epsilon_{\|}^{\frac{1}{2}}\,\tau\,\sin\phi\,\cos\phi}{(1 + \tau\,\sin^2\phi)^{\frac{3}{2}}} \tag{6.5}$$

We find numerically, using Runge-Kutta-Fehlberg method, solutions to the above equilibrium equation. These solutions are found to be essentially similar to the kink solutions permitted in static magnetic fields.

6.2.2 Kinks in combined magnetic and optical fields

We now consider the effect of the electrical field $\mathcal{E}$ of the light wave on kinks that are already present in the presence of an external magnetic field H. The different geometries which could be studied include the electric field of the light wave E being either parallel or perpendicular to the static magnetic field H with ϵ_a and χ_a being positive or negative.

We discuss only one geometry shown in figure 6.2 (b) where $\mathcal{E}$ is perpendicular to H and we have at E = 0 a splay-rich wall. We assume both ϵ_a and χ_a *to* be positive. The corresponding equation of equilibrium is

$$K\frac{\partial^2\phi}{\partial z^2} = \frac{I\,\epsilon_{\|}^{\frac{1}{2}}\,\tau\,\sin\phi\,\cos\phi}{(1 + \tau\,\sin^2\phi)^{\frac{3}{2}}} - \chi_a\,H^2\,\sin\phi\,\cos\phi \tag{6.6}$$

It is clear from equation (6.6) that the torque acting on the director due to the static

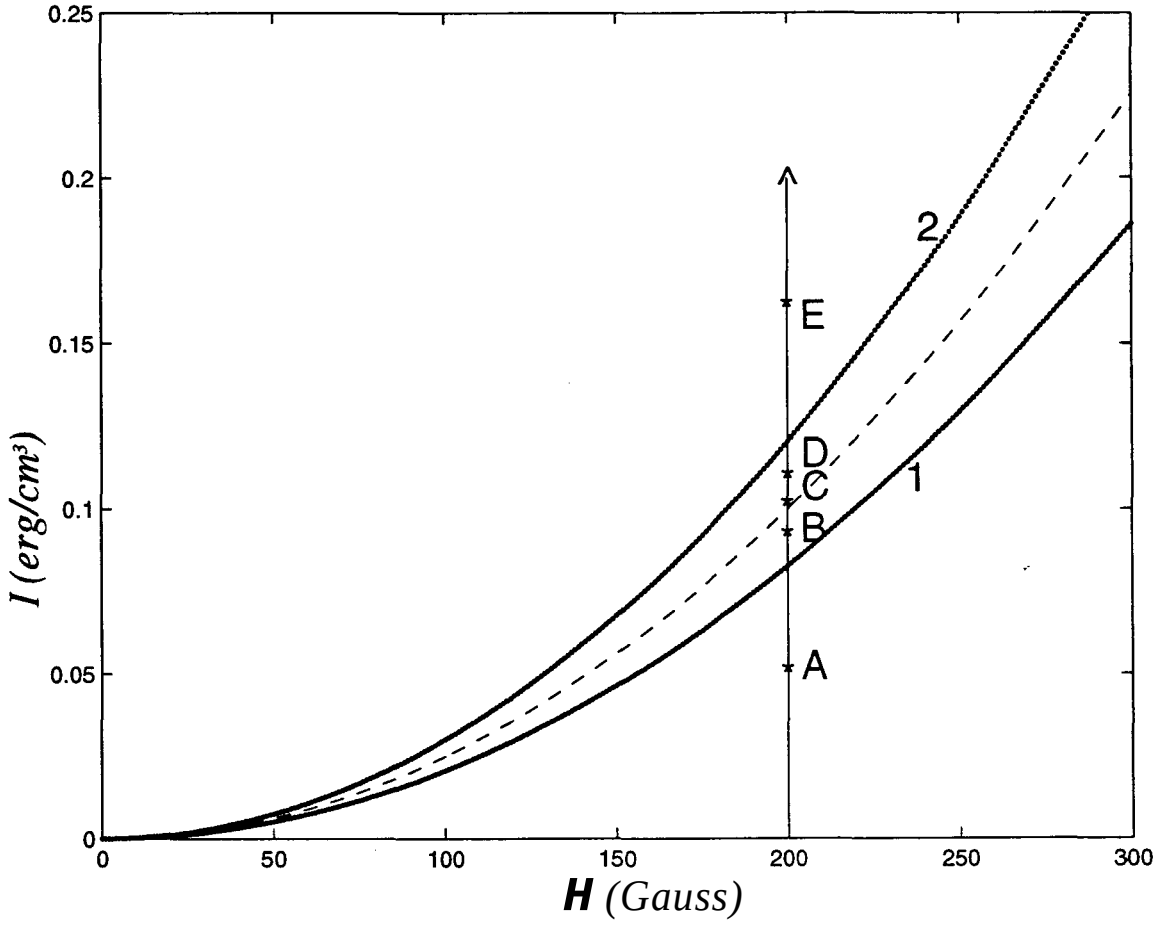

Figure 6.3: *Phase diagram for the kink state in a nematic. The dashed curve is a line of first order transition The dotted lines 1 and 2 are stability lines. Here I is the measure of intensity.* $\epsilon_{\|} = 2.89$, $\epsilon_{\perp} = 2.25$, $K = 10^{-6}$ *dyne. The A, B, C. D and E along the vertical line are points at which the kink solutions are obtained(see figure 6.4).*

magnetic field H opposes that due to the electric field $\mathcal{E}$ of the light wave.

Now we take up kink states that can exist in the same geometry. We solve equation (6.6) to get the permitted kink states. The phase diagram of transitions between different kink states is shown in figure 6.3. Interestingly, we find that the phase diagram for transition between different permitted kink states is the same as that for uniform states discussed in chapter 4. In terms of an effective potential $V(\phi)$ defined by:

$$V(\phi) = \frac{I\,\epsilon_{\|}^{\frac{1}{2}}}{(1 + \tau \sin^2\phi)^{\frac{1}{2}}} + \frac{\chi_a}{2} H^2 \sin^2\phi$$

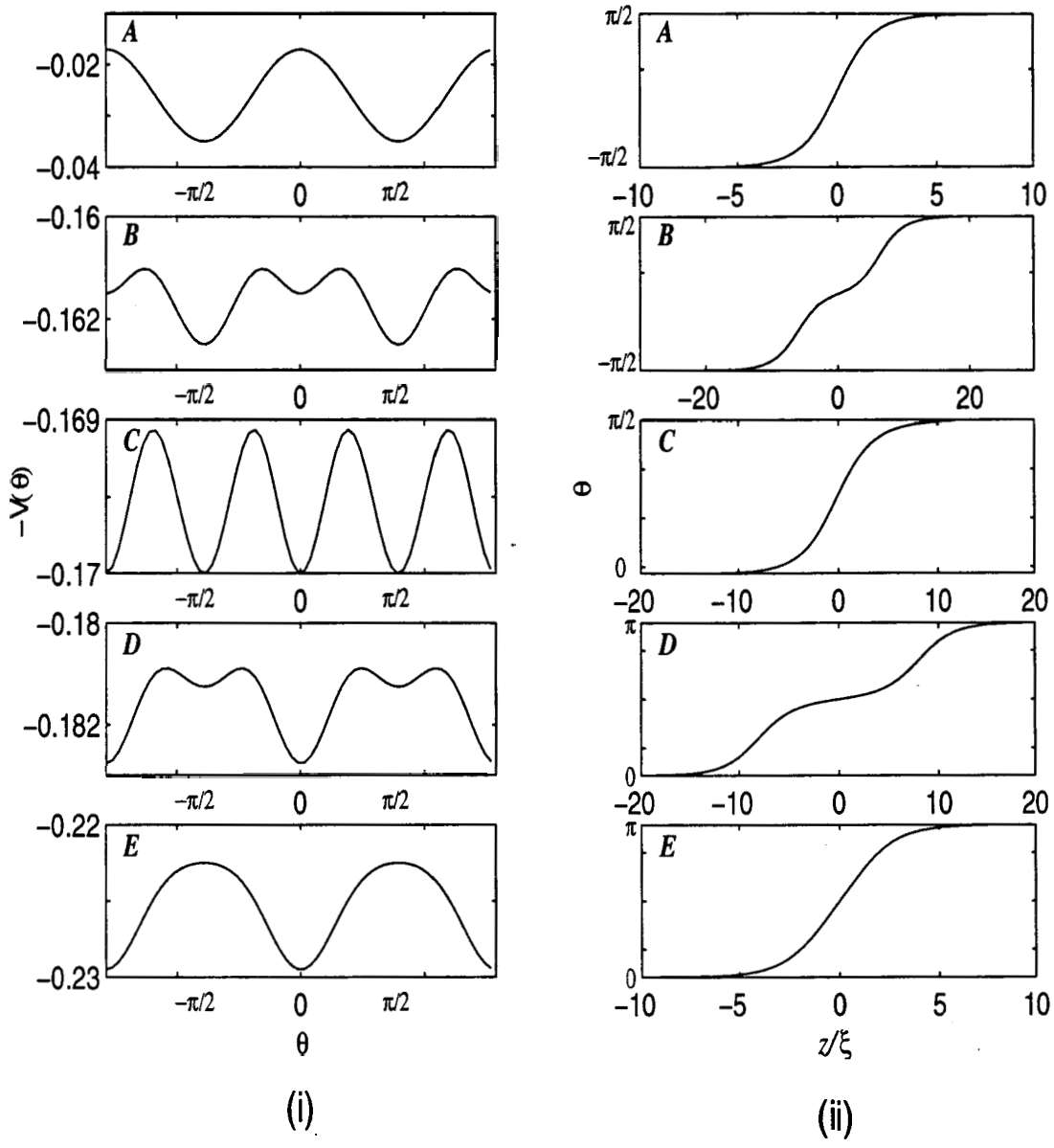

Figure 6.4: *(i) Negative of the effective potential V as a function of ϕ. (ii) Kink solutions. Here* 4 *is in radians and* $\xi = K/\chi_a H^2$, *the coherence length.*

Then equation (6.6) can be written as

$$K\frac{\partial^2\phi}{\partial z^2} = -\frac{\partial V}{\partial \phi}$$

The uniform states are given by the minima of $-V(\phi)$. The potential as a function of ϕ and the permitted kink solutions in regions **A,** B, C, D and E of the phase diagram are shown in figure 6.4 (i) and 6.4 (ii) respectively. In figure 6.5 we show the director profiles of the kink states permitted in these regions. The flat region in a kink profile corresponds to a local minima in − V or equivalently a metastable state. These are states with minima in the total free-energy functional but not global

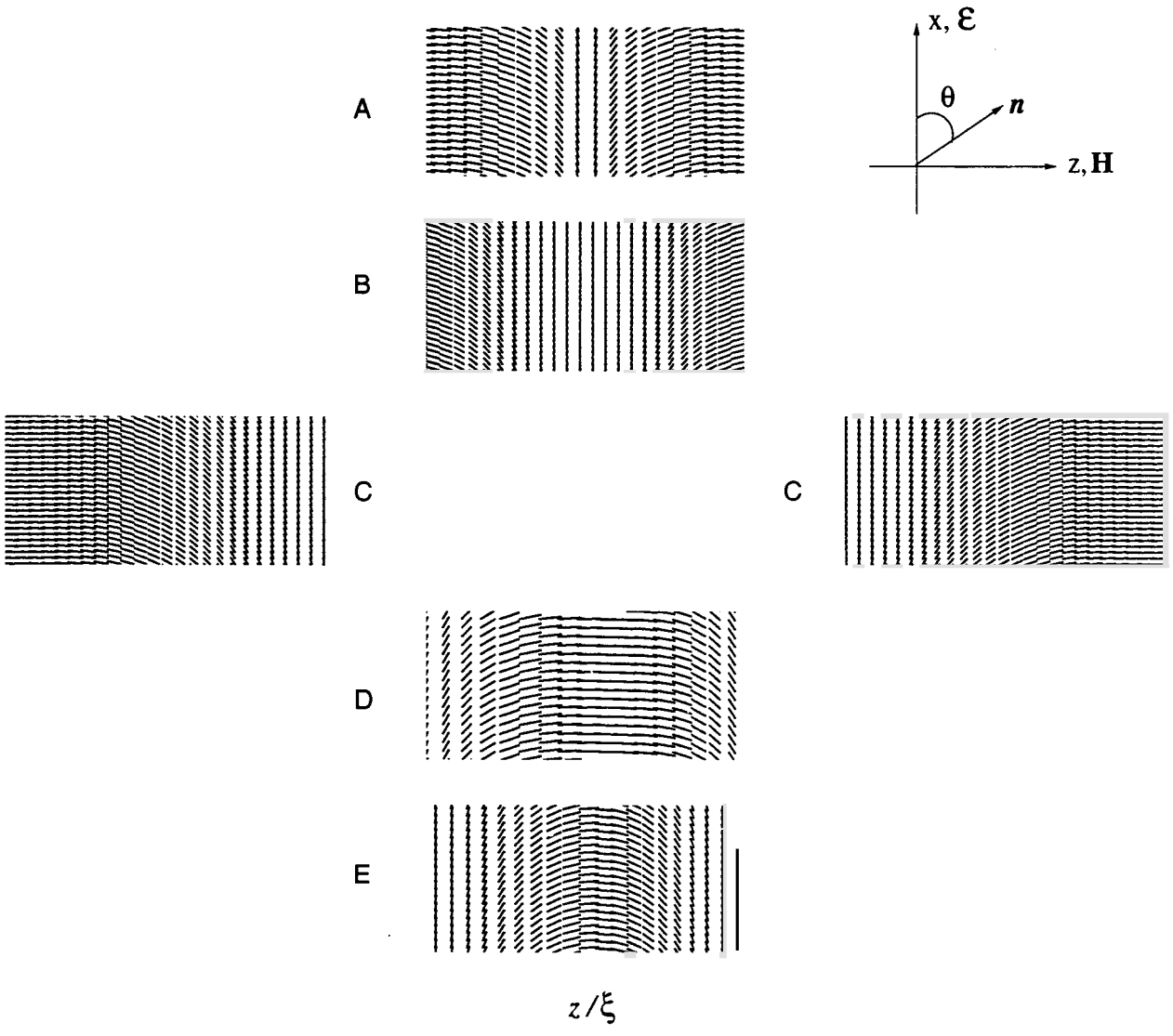

Figure 6.5: *Director configuration of the kink states permitted in the regions A, B, C, D and E of the phase diagram(figure 6.3).*

minima. As we go from region **A** to region E, the laser intensity **I** or consequently the electric field $\mathcal{E}$ increases in magnitude. We get a splay-rich kink in the region **A** while we end up with a bend-rich kink in the region E. There is a first order transition between these two kink states. On the dashed line two new kink states connecting $-\pi/2$ to 0 and 0 to $\pi/2$ become permitted solutions. This is unlike in a usual nematic in external static fields where the kink connects only 0 and π states. Hence, the scenario is like this: a $[(-\pi/2), \pi/2]$ splay-rich kink becomes unstable along the dotted line 1 and splits into a bound pair of $[-\pi/2, 0]$ and $[0. \pi/2]$ kinks linked by $\phi = 0$ uniform state. As **I** increases further the separation increases and it diverges to infinity as the dashed line is approached. On the other side of the dashed line the permitted kink solution is a bound kink pair of $[0, \pi/2]$ and $[\pi/2. \pi]$. Finally these two merge after the dotted line 2 is crossed to result in $[0, \pi]$ bend-rich kink.

These results are summarised in Table 6.1 along with the results for the uniform

Table 6.1: *The various Stable and Metastable states and the Kink statw in the different regions of the phase diagram shown in figure* 6.3

	Uniform State			*Kink State*	
Region	*Stable States*		*Metastable States*	*Topological Charge*	*Split Occurs at*
A	$-\pi/2$	$\pi/2$	-	π	-
B	$-\pi/2$	$\pi/2$	0	π	0
C	$\pi/2$	0	-	$\pi/2$	-
D	0	π	$\pi/2$	π	$\pi/2$
E	0	π	-	π	-

state. This depicts only one set of permitted solutions and not their symmetry related ones. Here the topological charge is the total change in the director orientation across the kink. The same results are obtained for the case of $\mathcal{E}$ parallel to H but with ϵ_a positive and χ_a negative.

6.3 Kink States in a Ferronernatic

An increase in the number of independent parameters in ferronematics leads to many possibilities. Here again the magnetisation M can be either parallel or antiparallel

to H with ϵ_a and χ_a being positive or negative. For the purposes of our discussion here we treat only the following two cases.

CaseI : $\mathcal{E}$ perpendicular to H. $\epsilon_a > 0, \chi_a < 0$ and M parallel to H

CaseII : $\mathcal{E}$ perpendicular to H, $\epsilon_a > 0, \chi_a > 0$ and M parallel to H

The other cases are similar to one or the other of these two cases. We discuss the first case in detail.

6.3.1 Ferronematic with negative diamagnetic anisotropy

In the case of kinks, different parts of the kink are at different orientations with respect to H. This causes the grains to migrate to regions of lower energy. Hence the grain concentration and thus f is not a constant. We then have to minimise the total free energy both with respect to f and ϕ to find the equilibrium director configuration.

Minimisation with respect to f leads to:

$$\mathrm{f} = C\, exp(\rho\, \mathrm{H}\, \sin\phi - 1) \tag{6.7}$$

where C is a constant of integration and $\rho = m\Omega/k_B\, \mathrm{T}$.

Since a kink connects two uniform(degenerate) states of same energy, the orientation ϕ_∞ of the uniform state at $z = \pm\infty$ can be obtained from a minimisation of the total free energy by neglecting the 'grain segregation'. With the boundary condition $\mathrm{f} = \overline{f}$ at $z = \pm\infty$ and $\phi = \phi_\infty$, equation (6.7) becomes:

$$\mathrm{f} = \overline{f}\, exp(\rho\, \mathrm{H}\, (\sin\phi - \sin\phi_\infty)) \tag{6.8}$$

Minimisation with respect to ϕ yields:

$$\begin{aligned} K\,\frac{\partial^2\phi}{\partial z^2} \;=\; & \frac{\mathrm{I}\,\epsilon_\parallel^{\frac{1}{2}}\,\tau\,\sin\phi\,\cos\phi}{(1+\tau\,\sin^2\phi)^{\frac{3}{2}}} + |\,\chi_a\,|\;H^2\,\sin\phi\,\cos\phi \\ & -m\,\overline{f}\,H exp(\rho\,\mathrm{H}\,(\sin\phi - \sin\phi_\infty))\,\cos\phi \end{aligned} \tag{6.9}$$

We solve this equation numerically to get the kink solutions. The kink structures will be sensitive to I and H. The kink states permitted in this case

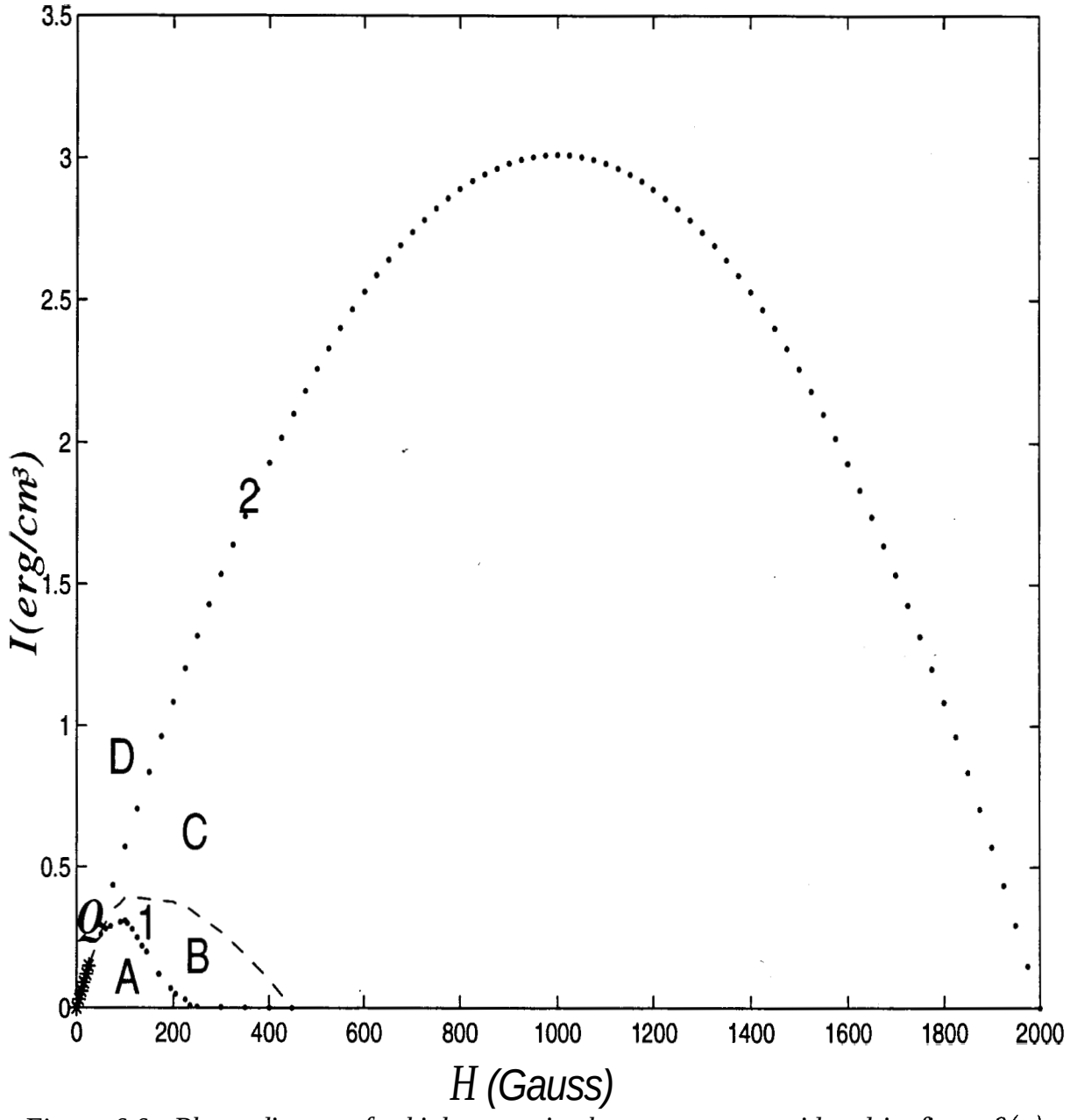

Figure 6.6: *Phase diagram for kink states in the geometry considered in figure 3(a). The starred curve represents a second order transition. The dashed curve is a line of first order transition. The dotted lines 1 and 2 are stability lines. Q is a tricritical point. Kink solutions are presented in regions A, B, C and D(see figures 6.7 and 6.8).*

are $[\pi/2, 5\pi/2]$, $[(\pi - \phi_o), \phi_o]$ and $[\phi_o, (3\pi - \phi_o)]$. The two quantities inside the square bracket gives ϕ at $z = \pm\infty$. The resulting phase diagram for the kink state is shown in figure 6.6. Up to a certain magnetic field, the order of transition between a $[\pi/2, 5\pi/2]$ kink and a $[(\pi - \phi_o), \phi_o]$ or $[\phi_o, (3\pi - \phi_o)]$ kink is second order. Beyond this field strength this transition becomes first order. Thus there is a *tricritical* point in the phase diagram. The dotted lines **1** and **2** are stability lines. These are

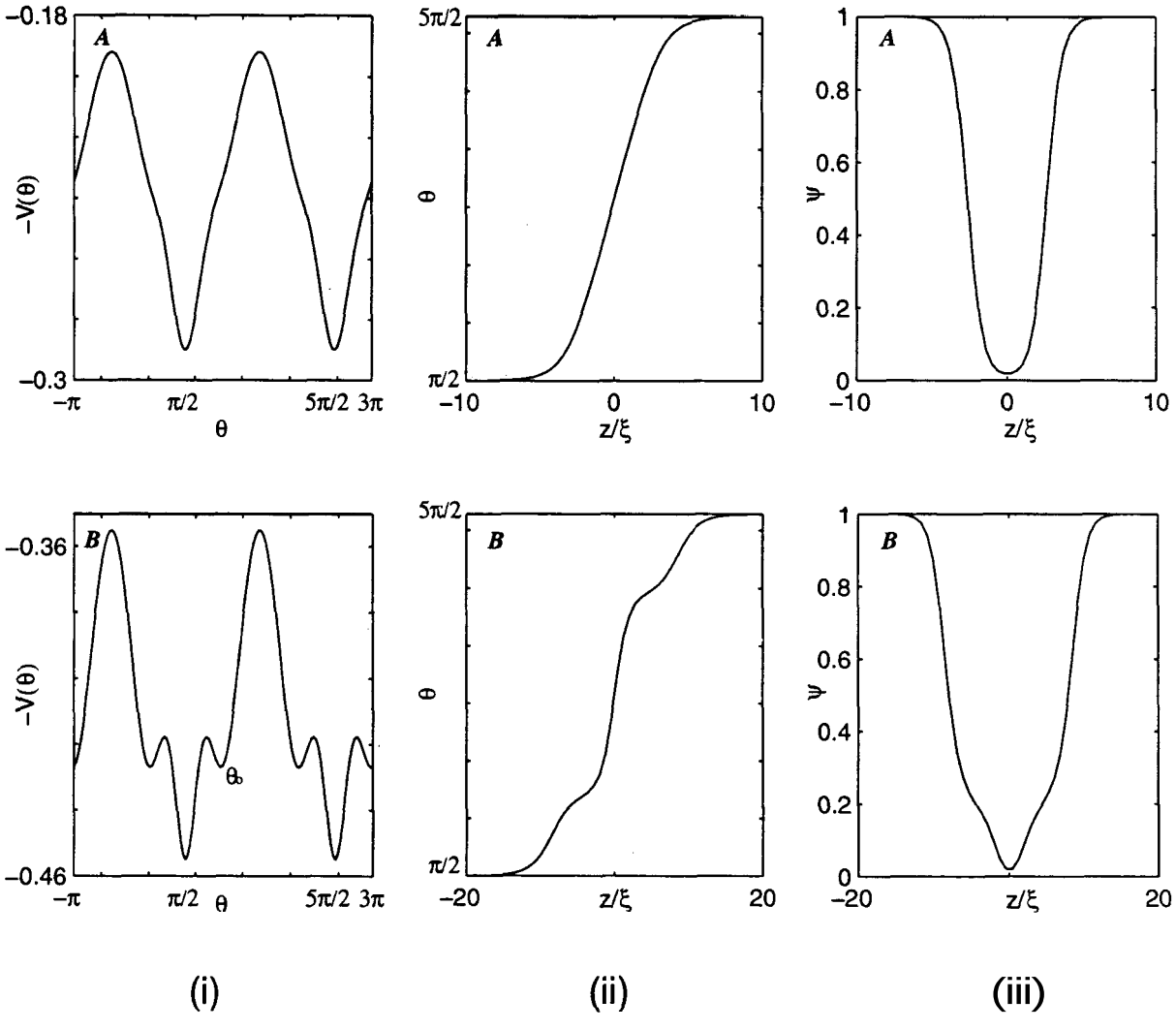

Figure 6.7: *(i) Negative effective potential as a function of ϕ, (ii) Kink solutions and (iii) Grain profiles in regions A and B of the phase diagram(figure 6.6). $\psi = f/\bar{f}$.*

lines about which a certain director orientation becomes metastable, i.e, the effective potential develops a local minima at this orientation. Along the dotted line **1,** the director orientations $(7\text{1-} - \mathbf{4,})$ and ϕ_o become metastable. Along the dotted line 2, the director orientations **7112**and $5\pi/2$ become metastable.

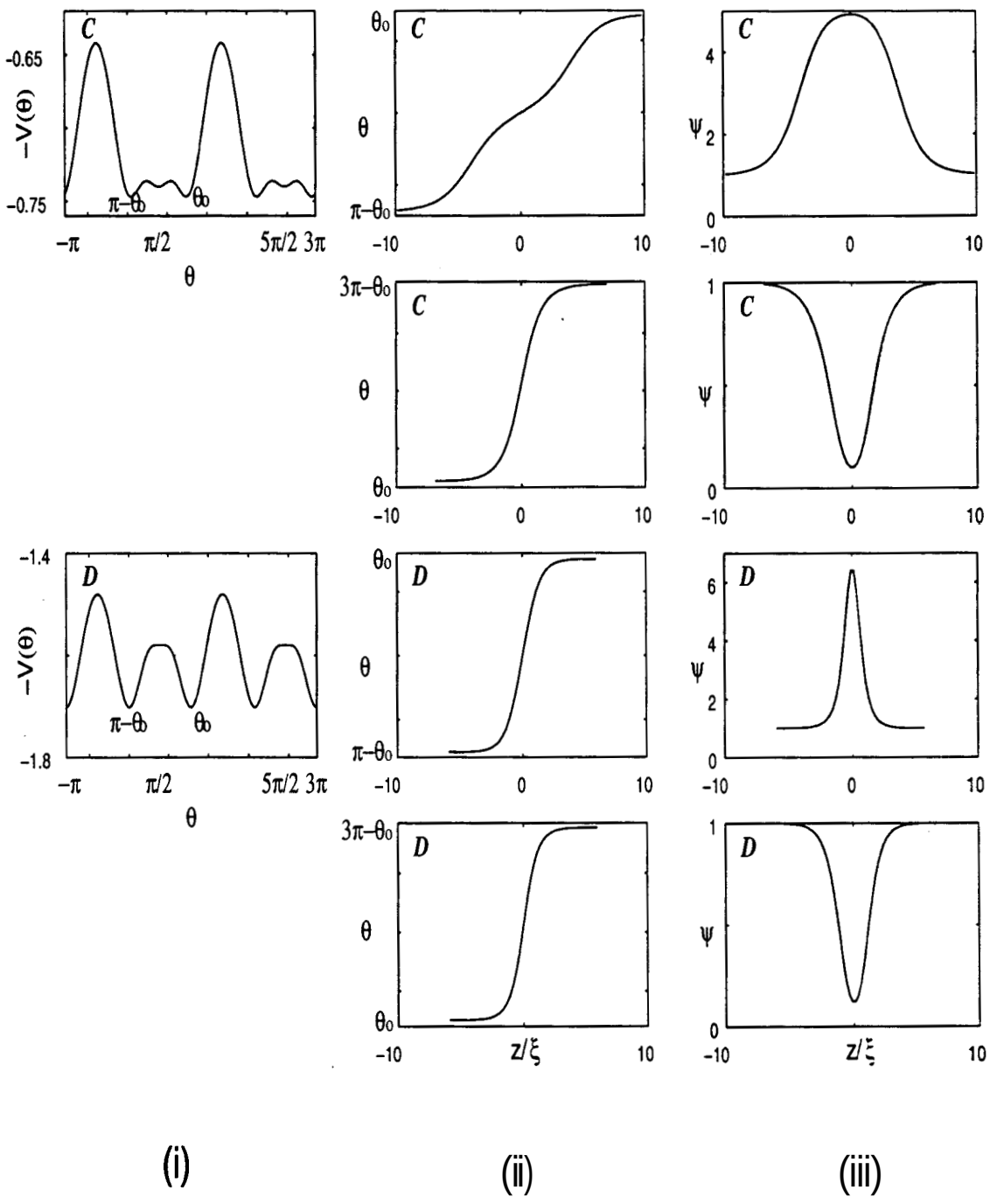

Figure *6.8: (i) Negative effective potential as a function of ϕ, (ii) Kink solutions and (iii) Grain profiles in regions C and D of the phase diagram(figure 6.6).*

In this case the effective potential is:

$$V(\phi) = \frac{I\,\epsilon_{\parallel}^{\frac{1}{2}}}{(1+\tau\,\sin^2\phi)^{\frac{1}{2}}} - \frac{|\chi_a|}{2}H^2\sin^2\phi + m\bar{f}H\exp(\rho H(\sin\phi - \sin\phi_\infty))$$

The figures *6.7* and *6.8* show respectively the potential, the kink states and the grain profile in the regions **A,** B, C and D of the phase diagram. In addition the phase diagram shows reentrance of a kink state as H is lowered. But this happens

only below a certain threshold value of the light intensity. We have summarised the

Table **6.2:** *The various Stable and Metastable states and the allowed Kink states in the different regions of the phase diagrams shown in figure* **6.6**

	Uniform State				Kink State		
Region	Stable States		Metastable States		Topological Charge	Split Occurs at	
A	$\pi/2$	$5\pi/2$	-	-	2π	-	-
B	$\pi/2$	$5\pi/2$	ϕ_o	$3\pi - \phi_o$	(i) 2π (ii) $3\pi - 2\phi_o$	ϕ_o -	$3\pi - \phi_o$ -
C	$-\phi_o$	ϕ_o	$\pi/2$	-	(i) $2\phi_o - \pi$ (ii) $3\pi - 2\phi_o$	$\pi/2$ -	- -
D	$\pi - 4$0	40	-	-	(i) $2\phi_o - a$ (ii) 377 $- 2\phi_o$	- -	- -

salient features of the uniform and the kink states in Table **6.2.** We have not depicted explicitly the symmetry related solutions.

6.3.2 Ferronematic with positive diamagnetic anisotropy

The phase diagram for the kink state obtained in this case is shown in figure 6.9. The starred line is a line of second order phase transition and the dotted line is a line of stability. The permitted kink states are $[\pi/2, 5\pi/2]$. $[(\pi - \phi_o), \phi_o]$ and $[\phi_o, (377 - \phi_o)]$. The phase diagram is richer here than in the previous cases. Here all the interesting features which we obtained in the previous cases are present in this one system. A small region in the phase diagram shows reentrant behaviour and there are regions where there are new stable states. It may be pointed out that interestingly, reentrant behaviour is not seen for the uniform states in the same case(see chapter 4). On the dashed line we find a transformation of a $[\pi/2. 5\pi/2]$ kink into a pair of kinks *viz.*, $[(\pi - \phi_o), \phi_o]$ and $[\phi_o, (3\pi - \phi_o)]$. This transformation is of second order at low **I** and H and first order at higher values of **I** and H implying the existence of a *tricritical* point on this line. The dotted lines **1, 2** and **3** arestability lines. Table **6.3** gives the essential features of the uniform and permitted kink states in the different regions of the phase diagram.. Here too we can generate symmetry related solutions from the ones given in the table.

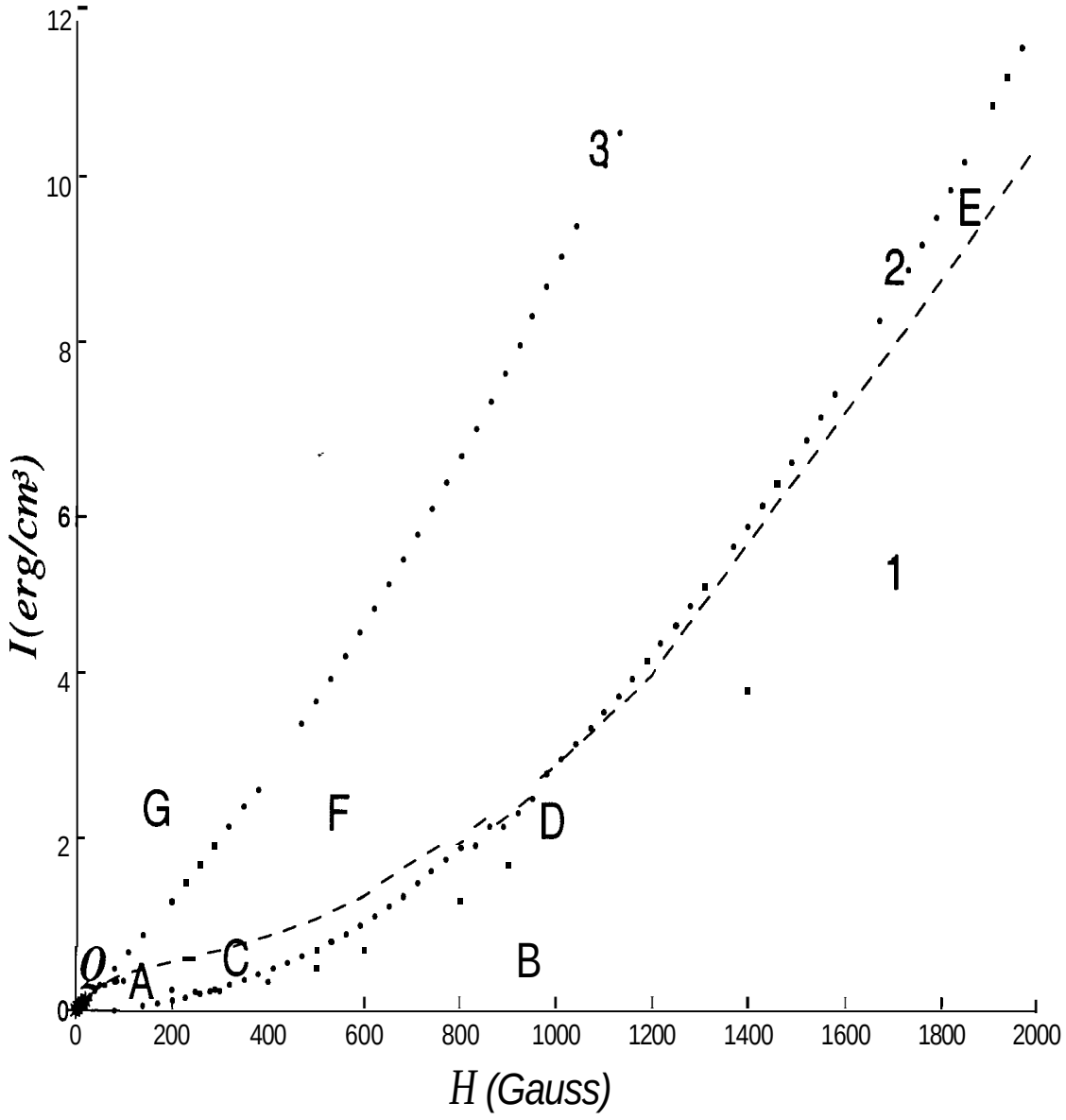

Figure 6.9: *Phase diagram for kink states in the geometry considered in figure 6.2 (b). Starred and dashed cuves are lines of second and first order respectively. Dotted lines 1, 2 and 3 are stability lines. Q is the tricritical point.*

Table 6.3: *The various Stable and Metastable states and the Kink states in the different regions of the phase diagram in figure 6.9*

	Uniform State					*Kink State*			
Region	*Stable States*		*Metastable States*			*Topological Charge*	*Split Occurs at*		
A	$\pi/2$	$5\pi/2$	-	-	-	2π	-	-	-
B	$\pi/2$	$5\pi/2$	-	$3\pi/2$	-	2π	-	$3\pi/2$	-
C	$\pi/2$	$5\pi/2$	-	ϕ_o	$3\pi-\phi_o$	(i) 2π (ii) $3\pi-2\phi_o$	ϕ_o -	$3\pi-\phi_o$ -	- -
D	$\pi/2$	$5\pi/2$	ϕ_o	$3\pi/2$	$3\pi-\phi_o$	(i) 2π (ii) $3\pi-2\phi_o$	ϕ_o -	$3\pi/2$ $3\pi/2$	$3\pi-\phi_o$ -
E	$\pi-\phi_o$	ϕ_o	$\pi/2$	$3\pi/2$	-	(i) $2\phi_o-\pi$ (ii) $3\pi-2\phi_o$	$\pi/2$ -	- $3\pi/2$	- -
F	$\pi-\phi_o$	ϕ_o	$\pi/2$	-	-	(i) $2\phi_o-\pi$ (ii) $3\pi-$ **24,**	$\pi/2$ -	- -	- -
G	$\pi-\phi_o$	ϕ_o	-	-	-	(i) $2\phi_o-\pi$ (ii) $3\pi-$ **24,**	- -	- -	- -

6.4 Effect of Boundaries

Finally, we remark on the influence of the boundaries in a finite sample. Two possible geometries are:

1: with boundaries parallel to the wall.

2: with boundaries perpendicular to the wall.

In case of boundaries parallel to the wall the director which is assumed to be anchored at the boundaries will influence the distortion in the bulk. Here the exercise of solving Maxwell's equations and equations of elastic equilibrium become boundary value problems which add to the computational complexity. In case of boundaries perpendicular to the wall we can show that a half strength defect has to exist at each boundary. This configuration affects the phase across a plane wavefront of light incident on the wall and hence does not conform to the geometrical optics approximation.

Bibliography

[1] L. Lam and J. Prost (Eds), Solitons in Liquid Crystals, (Springer-Verlag) 1991

[2] L. Lam, Chaos, Solitons and Fractals, **5(10)**, 2134 (1995)

[3] P. G. de Gennes and J. Prost, The Physics of Liquid Crystals (Oxford Science Publications) 1993

[4] S. K. Srivatsa and G. S. Ranganath, Phy. Rev. E **60**(**5**), 5639 (1999)

[5] N. V. Tabiryan, A. V. Sukhov and B. Ya. Zel'dovich, Mol. Cryst. Liq. Cryst., 136, 1 (1986)

[6] H. L. Ong, Phys. Rev., **A28,** 2933 (1982)

Chapter 7

BEAM PROPAGATION

To read the letters of the cosmic script
And study the body of the cosmic self..
-Sri Aurobindo in Savitri, -p 266

7.1 Introduction

At small intensities of the laser beam the refractive index of the medium is independent of the intensity. For higher intensities the refractive index becomes a function of the field strength. In fact, the classical Kerr nonlinearity leads to a nonlinear refractive index which is proportional to the laser intensity. If the medium is absorbing we also have the process of thermal indexing. In chapter 2 we have shown that in liquid crystals we have in addition to the nonlinear processes like *director reorientation, laser suppression of the director fluctuations*, and *laser induced tilt angle in smectics*. In the earlier chapters we studied the effect of laser propagation resulting in structural changes in liquid crystals. In this chapter we study the effect on the laser beam itself due to these inherent nonlinearities of liquid crystals. We consider the laser beam propagation in the two regimes: (i) the beam width is very large compared to the wavelength of laser so that natural self-diffraction of the laser beam can be neglected and (ii) the beam width is small enough for self-diffraction to become important. In the latter case we look at the possible existence of optical solitons in the low absorption limit. As discussed in chapter 1 there could be either temporal or spatial solitons. Here we consider only spatial solitons for rea-

sons to be made clear soon. We have worked out the structure of the spatial solitons due to non-Kerr nonlinearities. Here we briefly recount the structure of a spatial soliton. In spatial solitons, if the nonlinearity is positive, an incident plane wavefront becomes a concave wavefront. This leads to focusing of the beam. On propagation, the beam width continues to decrease. When the beam width becomes comparable to the wavelength of light, optical diffraction sets in. This leads to scattering of the beam. At appropriate intensity it can happen that the diffraction of the beam is exactly nullified by the focusing effect due to the nonlinearity. In such cases the laser beam travels without change of shape and is called an *optical spatial soliton* [1]. It should be mentioned that usually the soliton formation length is about a few kilometers length in the usual nonlinear media [2, 3]. In liquid crystals since, the nonlinear coefficient is a million times larger the soliton formation length is very small. In fact, it can be of the order of few μm. Further, in usual Kerr media the formation of spatial solitons require higher intensities neccessary to compensate for the large self-diffraction effects.

Now we briefly indicate why temporal solitons are not being considered in our studies. Lam et. al.,[2, 4] were probably the first to draw attention to the optical solitons in liquid crystals. They suggested that the optical nonlinearity due to laser induced director reorientation results in the formation of temporal and spatial solitons. Rodriguez et. al., [5, 6] also studied this problem in the waveguide geometry. These authors, however, did not take into account the inevitable director relaxation process in liquid crystals. Director relaxation is a very slow process and has time scales of the order of a few milliseconds to seconds. However, the optical pulse propagates very fast, in fact, with the velocity of light in the medium. Since the field is non-zero only for a very short duration and the medium does not respond to the field within that time interval there are conceptual difficulties in accepting the suggested solutions for the temporal solitons. In contrast, the process'of director reorientation does not lead to such conceptual difficulties in the case of spatial solitons. It may be mentioned in this context that, Warenghem et. al., [7] have provided experimen-

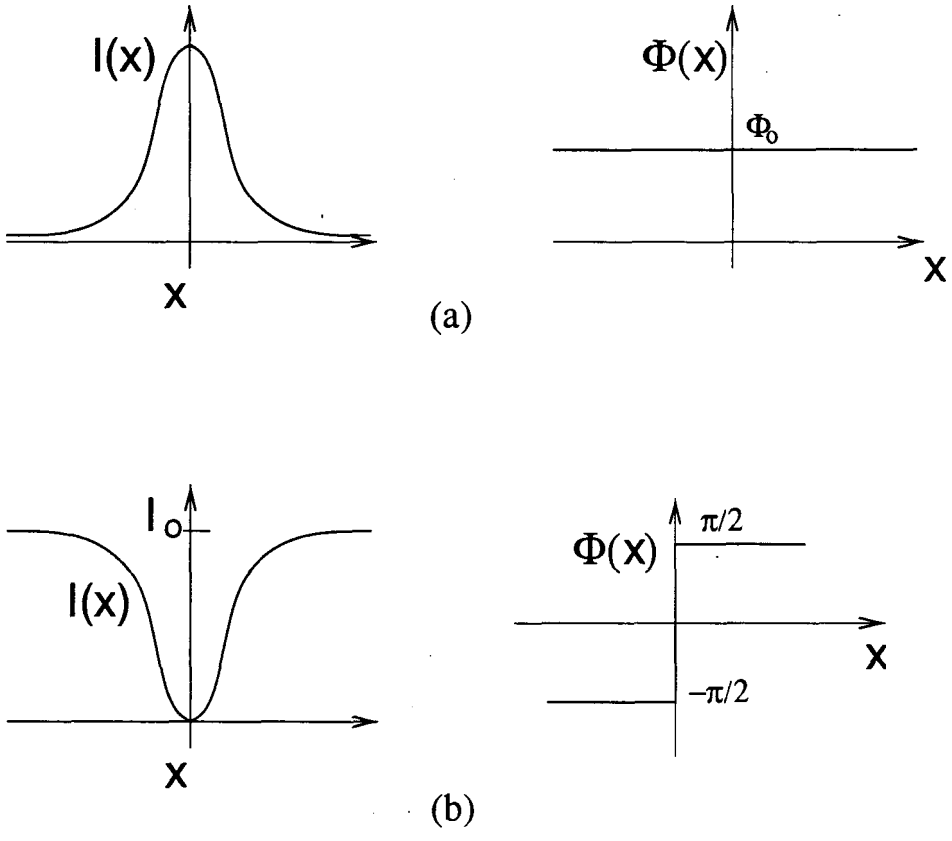

Figure 7.1: *The profile of (a) a bright soliton and (b) a dark soliton along with the phase of the propagating wave is shown here. $I(x)$ is the intensity profile across the wavefront and $\Phi(x)$ is the phase of the propagating wave. I_o is the intensity of the background in the case of dark soliton. In the case of the dark soliton we have a phase jump of π*

tal evidence for the existence of spatial solitons in liquid crystals. In liquid crystals the nonlinear coefficient due to thermal indexing can be both positive or negative depending on the geometry and the polarisation of the laser field. If laser absorption is weak or sample thickness is small then we can neglect to a good approximation the reduction in the laser intensity during its propagation in the sample. We work out solitons in this limit for this nonlinearity which is also known in the literature as the $thin - film$ approximation[8]. In fact, in the presence of thermal indexing alone, Bertolotti, et. al., [9] have found out numerically that the stable soliton like propagation is possbile over small distances in glass fibres. Here, the rigorous solution requires one to solve for both the temperature profile and the field amplitude simultaneously. The temperature profile is obtained from the thermal diffusion equation and thus this process provides a diffusive nonlinearity. It has been stated already that in

liquid crystals the nonlinearity could be positive or negative. When this nonlinearity balances exactly the diffraction effect we get either a 'bright' soliton or a 'dark' soliton [10] depending upon the sign of the nonlinearity. Their profiles are shown in the figure *7.1.* Interestingly, in the case of a 'dark' soliton we have a phase jump of π.

7.2 Beam Modulation and Thermal Indexing

If the beam width is very large compared to the wavelength of the laser then to a very good approximation we can ignore self-diffraction effects. The beam diameter inspite of self-focusing may yet be much bigger than the wavelength. In this section we consider nematic liquid crystals in such situations.

7.2.1 Uniform nematics

Let a linearly polarised beam propagate perpendicular to the director with its electric vector parallel to it. In this geometry we get an optical nonlinear effect due to the suppression of the director fluctuations. If the material is also weakly absorbing we also get thermal indexing since the temperature of the system locally increases leading to a decrease in the local refractive index for this vibration. The change $\delta T(I)$ in temperature is proportional to the local laser intensity, I. Hence the change $\delta\mu(I)$ in the refractive index is also proportional to *I!* The increase in the refactive index for light polarised along the director due to the laser suppression of director fluctuations can be easily worked out from equation *(2.11)* of chapter *2.* We get:

$$\begin{aligned} \mu_{nl}(I) &= k_B T \sqrt{\frac{\epsilon_a^3}{2\pi^3 K^3}}\ \sqrt{I} \\ &= \eta_1 \sqrt{I}, \eta_1 = k_B T \sqrt{\frac{\epsilon_a^3}{2\pi^3 K^3}} \end{aligned} \tag{7.1}$$

and the thermal indexing is similar to the Kerr process. Its effect on the refractive index is negative as made clear in chapter 1. Since these two nonlinear processes compete with each other the change in the refractive index' in the presence of both these nonlinearities can be written as:

$$\delta\mu(I) = \eta_1 \sqrt{I} - \eta_2 I, \eta_2 = \frac{d\mu}{dT}\left(t^2\chi/\pi^2\kappa\right)\ I \tag{7.2}$$

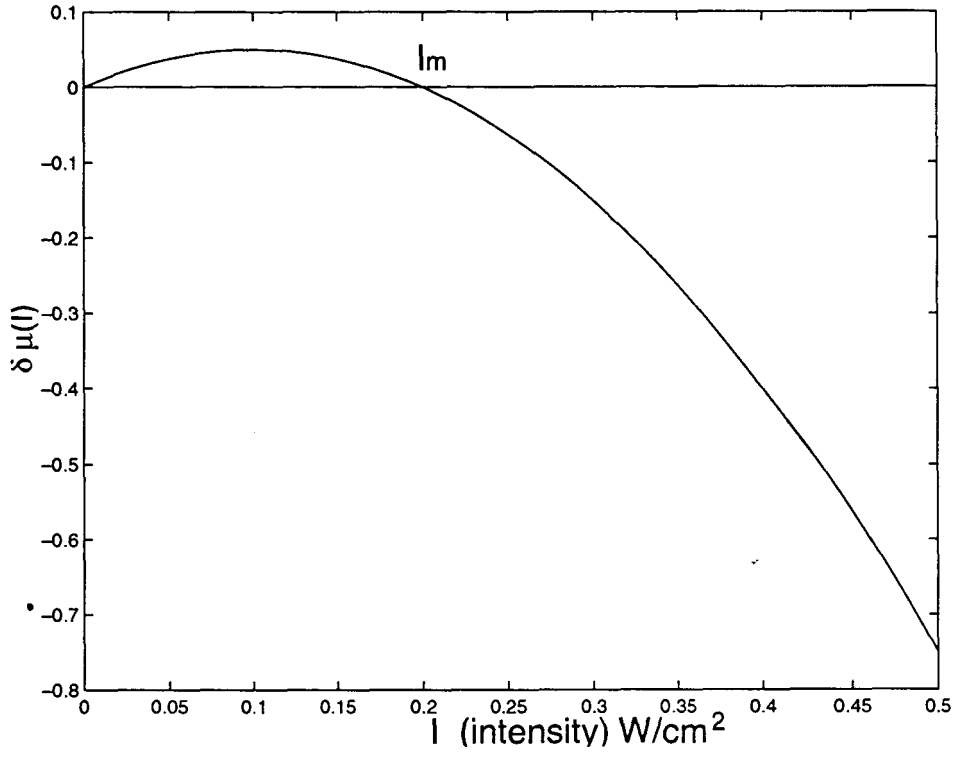

Figure 7.2: *Variation of the refractive index when both the processes of the suppression of the director fluctuations and the thermal indexing are operating in a nematic liquid crystal. I, is the intensity at which the nonlinearity changes its sign.*

The net refractive index change is as shown in figure 7.2. The change $\delta\mu$ reaches a maximum and becomes zero again at an intensity $I_{zz} = \eta_1^2/\eta_2^2$. Below this intensity the process of laser suppression of director fluctuations dominates and $\delta\mu$ is positive while above the intensity I, the process of thermal indexing dominates and $\delta\mu$ is negative. The positive nonlinearity leads to self-convergence and the negative nonlinearity to self-divergence of a parallel incident laser beam.

(i) **Thick samples** :

(a) *Polarised beam* Let us chose the intensity **I** of the incident beam less than I_{zz}. Hence, initially the beam converges. This increases the intensity in the beam due to reduction of the cross-section of the beam. **As** the intensity increases and becomes greater than I_{zz} then the beam starts diverging. This leads to an increase in the cross-section of the beam and hence to a reduction in its intensity. Further, at some large width, intensity falls below I, and again the beam starts converging. The process repeats indefinitely leading to a periodic modulation of the beam width

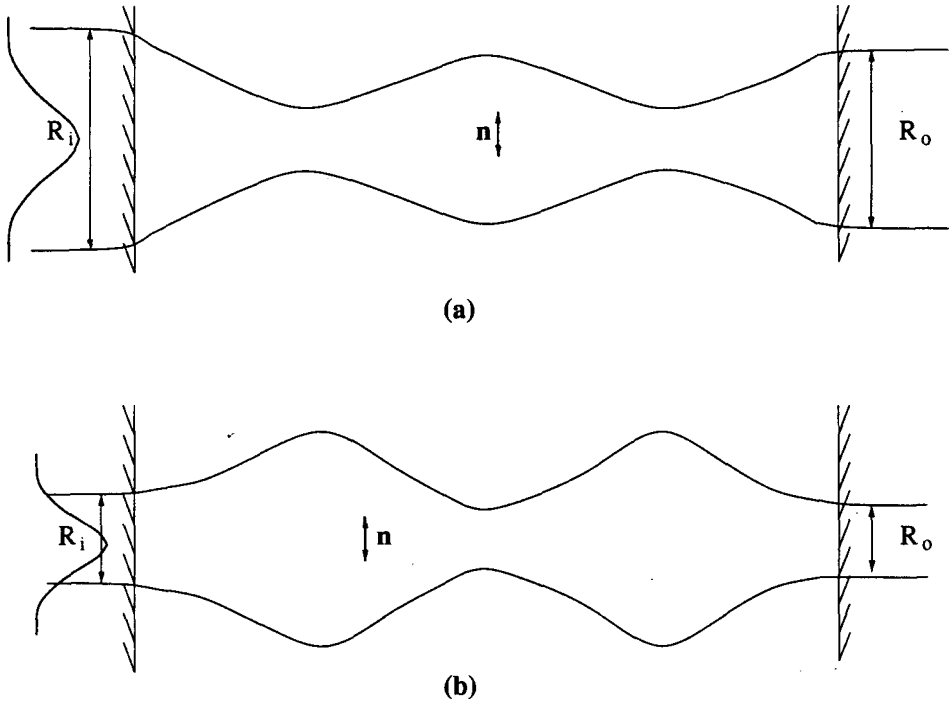

Figure **7.3:** *(a) The modulation of the beam width when the intensity $I < I_m$. The beam initially converges and repeatedly undergoes divergence and convergence. (b) The beam width initially increases on entrance when the intensity is $I > I_m$. On propagation, the beam width periodically increases and decreases.*

along the direction of propagation. This is schematically depicted in figure **7.3** (a). The same is to be expected even in case of an incident beam with its intensity greater than I. Here the beam width evolution with distance is as shown in figure **7.3** (b).

(b) *Unpolarised beam* : Laser beams with electric fields along and perpendicular to the director are the eigenwaves in a nematic [11]. As already said the nonlinear coefficient due to thermal indexing, for the wave propagating in a medium with its electric vector parallel to the director, is negative and for the orthogonal component it is positive. Hence, the component parallel to the director is diverging while the component perpendicular to the director is focusing. Any incident vibration gets resolved into these eigenstates. In the case of unpolarised light the two eigenstates will be equally intense. When such a beam traverses through a nematic then due to the optical nonlinearity we find that both the components are affected. The

component parallel to the director undergoes the same tranformations as already described. For the component perpendicular to the director η_1 is negative and η_2 is positive. Hence, if the parallel component focuses initially on entry into the medium, the orthogonal component diverges initially.

(ii) Thin **samples** :

(a) *Polarised beam* : This case leads to either focusing or divergence of the beam at the exit. This crucially depends on the initial intensity of the incident beam. If the intensity is lesser than I_m then the beam is focused on exit. If the intensity is greater than I_m then the beam is divergent on exit.

(b) *Unpolarised beam* : In this case when such a beam traverses through a thin nematic then due to the optical nonlinearity we get a central bright spot polarised parallel to the director, surrounded by a divergent beam polarised perpendicular to the director.

7.2.2 Hybrid nematic

Non-uniform director configuration also affects the beam characteristics. To illustrate this situation we consider propagation in a hybrid aligned nematic whose director configuration is shown in figure 7.4. At one of the bounding glass plates the director is homogeneously aligned i.e., parallel to the surface and at the other bounding glass plate the director is homeotropically anchored i.e., perpendicular to the surface. In the intervening space the director smoothly goes over from one alignment to the other. In figure 7.4 (a) the laser beam is polarised parallel to the director and is incident on the plate with the homogeneous alignment. We assume optical anisotropy, ϵ_a to be small that we can ignore laser effects on the director. We consider only thermal indexing. Then the beam to start with, will diverge. As it propagates, due to thermal indexing, the negative nonlinear coefficient decreases in magnitude and changes sign at a particular point and becomes positive beyond it. After this stage the beam converges. It is thus possible, by a suitable choice of the thickness, birefringence and absorption coefficients to design a cell where the beam width on emergence is equal to

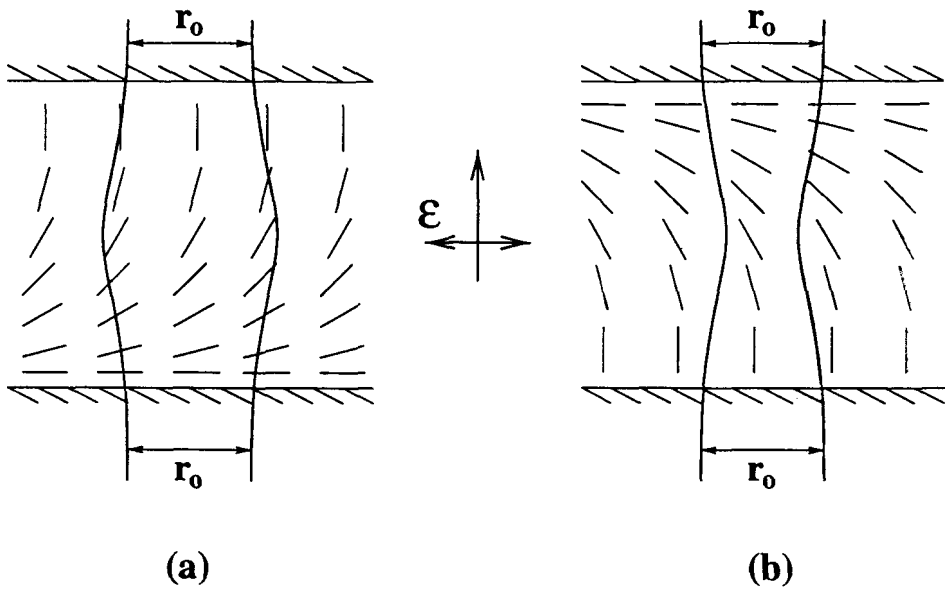

Figure 7.4: *Beam transformations in a hybrid aligned nematic. The electric vector is in the plane of director distortion. The beam width is the same at both the exit and entrance points. (a) Laser incident on the homogeneously aligned surface. (b) Laser incident on the homeotropically aligned surface.*

the width it had at the entrance point. On the other hand, in figure 7.4 (b) the beam is incident on the plate with homeotropic alignment with the electric field in the plane of the director distortion, the beam initially converges which eventually diverges on further propagation. Again it is possible to choose the material parameters such that the beam width is the same at the entrance and the exit ends of the sample.

7.2.3 Flexoelectric nematic lattice

It is known that a uniform nematic subjected to a static electric field. under certain conditions, exhibits an instability leading to an one dimensional periodic planar splay-bend lattice [12]. The wavevector of periodicity is always along the direction perpendicular to the static electric field. A schematic representation of this is shown in figure 7.5 (a). It has alternate regions of splay-rich and bend-rich deformations.

Let a linearly polarised beam with its electric vector in the plane of the director distortion propagate along z-axis, the direction of.lattice wavevector. We shall again assume that ϵ_a for light is so small that the laser field will nor alter the director configuration. We consider only thermal indexing. Since thermal indexing

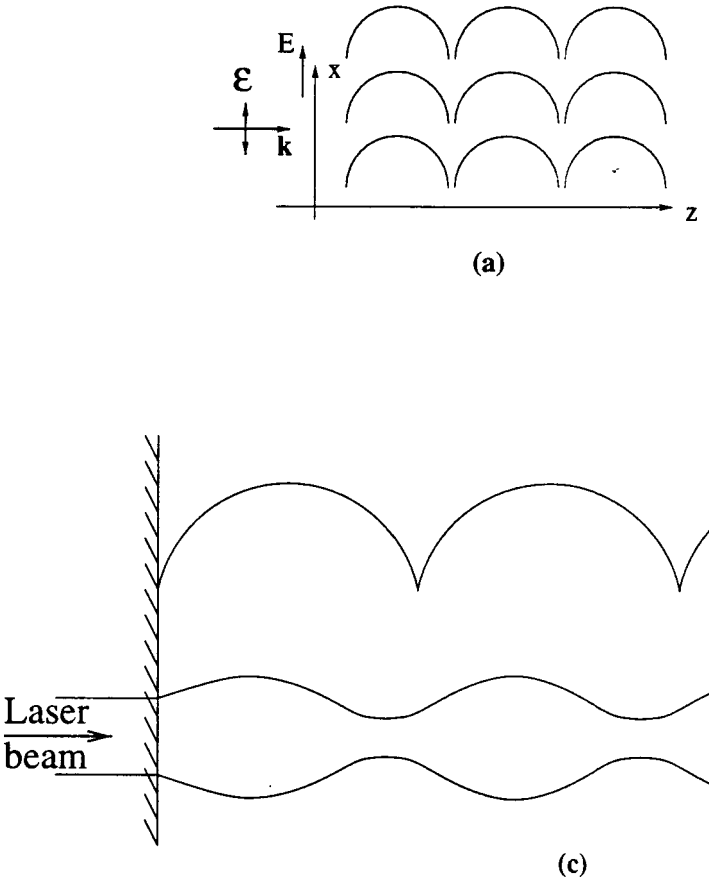

Figure **7.5:** *(a) The flexoelectric lattice in the presence of a static electric field E. The periodicity is along the z direction perpendicular to the electric field. (b) Periodic variation of the beam width due to periodic opposing nonlinearities induced by thermal indexing in a flexoelectric lattice.*

is dependent on the angle between the electric vector of the laser and the director, it leads to a nonlinear coefficient which is periodic with the period of the lattice. This leads to a periodic convergence and divergence of the incident beam leading to novel transformation of an otherwise parallel beam into a beam of modulated width. These modulations are schematically shown in figure 7.5 (b).

7.3 Structure of Spatial Solitons

7.3.1 Due to laser suppression of director fluctuations

The nonlinear optical coefficient due to laser suppression of director fluctuations is positive. We note that the same process affects even the in-plane fluctuations in the c-director of a smectic C liquid crystal when the electric vector of the laser is parallel to the c-vector.

We consider the soliton solution due to this nonlinearity alone. The nonlinear Maxwell equation in the slowly envelope approximation simplifies to the nonlinear Schrodinger equation (see section 1.7):

$$2ik_{\circ}\mu_{\circ}\frac{\partial\mathcal{E}(X,Z)}{\partial Z}+\frac{\partial^2\mathcal{E}(X,Z)}{\partial X^2}+2k_{\circ}^2\mu_{\circ}\mu_{nl}(I)\,\mathcal{E}(X,Z)=0 \qquad (7.3)$$

where $\mathcal{E}$ is the envelope of the electric field, Z is the distance along the direction of propagation, X is the transverse coordinate, $\mu_{\circ}$ is the linear refractive index and $k_{\circ}$ is the wavevector of the laser beam. In the present case the local nonlinearity is introduced by the function $\mu_{nl}(I)=\eta_1\sqrt{I}$. The soliton solution for this situation is given by

$$\mathcal{E}(X,\mathrm{Z})=\psi(X)exp(i\nu Z)$$

$$\psi(X)=\left(\frac{3A}{2B}\right)\frac{1}{\cosh^2(\sqrt{A}\,X/2)} \qquad (7.4)$$

where $\boldsymbol{A}=2\mu_{\circ}k_{\circ}\nu$ and $\boldsymbol{B}=2k_BT\mu_{\circ}k_{\circ}^2\sqrt{\frac{\epsilon_a^3}{2\pi^3K^3}}$. $\boldsymbol{A}$ beam of this amplitude profile travels unaltered through the medium. This is called a spatial soliton. This solution has to be compared with

$$\psi(X)=\left(\frac{2a}{b}\right)\frac{1}{\cosh(\sqrt{a}\,X)}$$

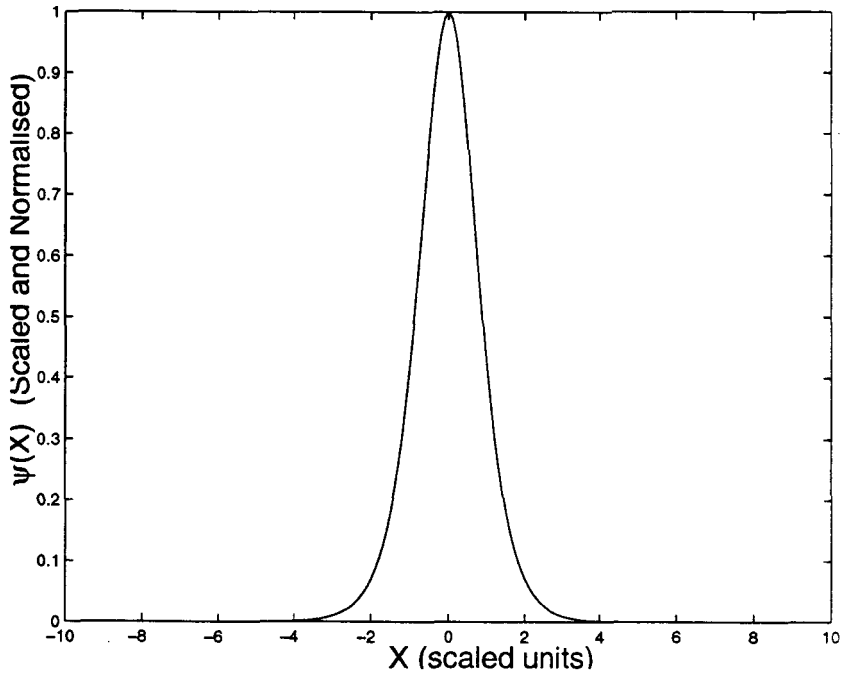

Figure 7.6: *A typical bright soliton profile when laser suppression of the director fluctuations alone acts.* $X = k_o x$ *is the scaled transverse coordinate.* $\psi(X)$ *is the scaled amplitude of the optical field.*

obtained in the case of usual Kerr nonlinearity.

This nonlinearity given by η_1 is positive and hence we get a bright soliton. A typical bright soliton obtained in such a case is depicted in figure 7.6. The above nonlinearity is of non-Kerr type and as said in chapter **1** it leads to only a solitary wave [10]. We have assumed here a local response of the medium to the laser field i.e., changes in the order parameter at different points are uncorrelated.

7.3.2 Due to laser induced tilt angle in smectics

It has been pointed out in chapter **3** that a laser induced change in the tilt order parameter in smectic liquid crystals again leads to large optical nonlinearities. The nonlinearity here is comparable to the giant optical nonlinearity due to the director reorientation [13, **14,** 15]. In smectic ***A*** the laser induced tilt angle is possible beyond a threshold intensity(chapter 3) and the correction to the refractive index is positive. The magnitude of the nonlinear coefficient depends on the direction of propagation and the polarisation of the laser beam. We recall here some aspects of this process

which are important for the discussions in this section. Their essential features are shown in figure 7.7. In the geometry shown in the figure 7.7 (b) and 7.7 (c) both the

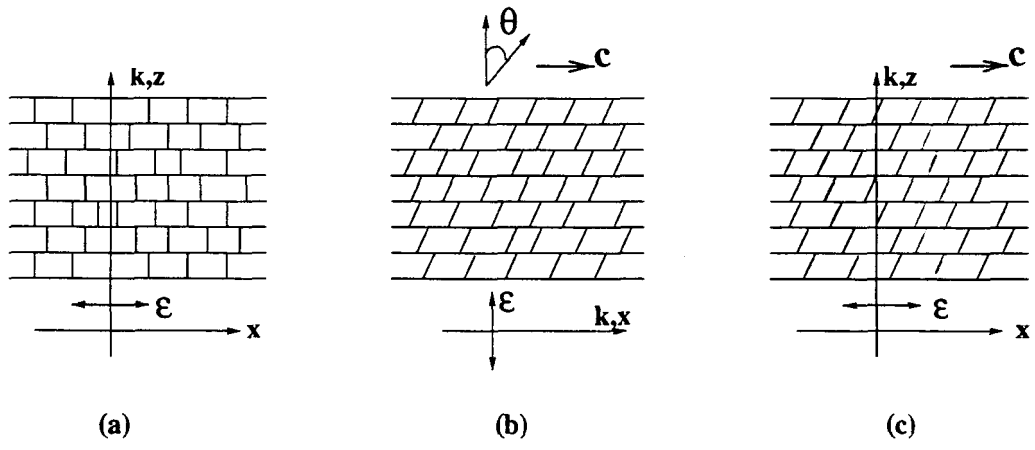

Figure 7.7: *(a) Geometry showing smectic A liquid crystal with the laser propagating parallel to the layer normal and the electric vector parallel to the layers. The molecular tilt is induced only beyond a particular intensity leading to a threshold type nonlinearity. (b) Geometry showing smectic C liquid crystal with the laser propagating parallel to the layers and the electric vector perpendicular to the layers. The molecular tilt becomes zero beyond a particular intensity thus leading to a satumble type nonlinearity and laser suppression of c-director fluctuations exist. (c) Geometry showing smectic C liquid crystal with the laser propagating parallel to the layer normal and the electric vector parallel to the layers along the c-director. The molecular tilt in creases with increasing intensity and also the in-plane c-director fluctuafions are suppressed.*

process of laser suppression of the c-director fluctuations and laser induced change in the tilt angle exists while in the geometry shown in the figure 7.7 (a) and 7.7 (b) only the process of laser induced tilt change operates. We consider two geometries. In the first, light propagates in a smectic *A* perpendicular to the layers with the electric vector of the laser beam parallel to the layers(see figure 7.7 (a)). In the second geometry, light propagates in a smectic C parallel to the layers and polarised perpendicular to the layers and in the plane of the tilt(see figure 7.7 (b)). These two cases are associated with different types of nonlinearities leading to a rich class of solitons. For a self-consistent solution of the Maxwell wave equation, the tilt angle should be obtained by minimising the total free-energy density. The corresponding free-energy density in terms of the tilt angle 6 is given by [8]:

$$\mathcal{F} = \mathcal{F}_o + \alpha' \theta^2 - \alpha'' I \theta^2 + \beta \theta^4 + \textit{higher order terms} \qquad (7.5)$$

+coupling terms

Here $\alpha' = \alpha_o(T - T_{AC})$, with T_{AC}, the smectic A-smectic C transition point and $\beta(> 0)$ are phenomenological constants in the free-energy density, $\alpha'' = \epsilon_a/16\pi c$, c being the velocity of light and ϵ_a is the dielectric anisotropy. The nonlinear coefficient here depends on the geometry i.e., the direction of propagation and the polarisation of the beam. If we make the parameter α in the free-energy density expression (7.5) zero by going to T = T_{AC}, then the nonlinear function $\mu_{nl}(I)$ is the same as Kerr type nonlinearity. In principle, we can effectively get the same result by applying a static magnetic field along the layers. This Kerr nonlinearity possesses a true soliton solution which must be distinguished from a solitary wave. We consider three geometries as depicted in figure 7.7 and which yield three different types of nonlinearities leading to three different types of soliton solutions.

(i) : In smectic A, near the smectic A to smectic C transition only the laser induced tilt nonlinear process is relevant. The geometry is shown in figure 7.7 (a). As the tilt angle is induced only beyond a particular intensity, this is of the threshold type nonlinearity [10]. The nonlinear function $\mu_{nl}(I)$ is given by:

$$\mu_{nl}(I) = \begin{cases} 0 & , \quad I < I_{th} \\ \frac{\epsilon_a}{2\mu_{\|}^2 \beta}\left(\frac{\epsilon_a I}{8\pi c} - \alpha\right), & I > I_{th} \end{cases}$$

The soliton solution with this nonlinearity is given by:

$$\psi(X) = \sqrt{\frac{2A_1}{B_1}}\,\frac{1}{\cosh(\sqrt{A_1}X)} \qquad (7.6)$$

where $A_1 = 2k_o\mu_\perp\nu + \frac{\alpha\epsilon_a}{2\mu_{\|}^2\beta}$ and $B_1 = \frac{k_o^2\mu_\perp\epsilon_a^2}{8\pi c\mu_{\|}^2\beta}$. Here $\mu_{\|}$ and $\mu_\perp$ are the refractive indices parallel and perpendicular to the nematic like director in the uniaxial approximation. Note that the width of the soliton is a function of the parameter v and the parameters are unlike the similar soliton discussed earlier in section 7.3.1

(ii) : In smectic C liquid crystals, in the geometry shown in figure 7.7 (b) again only the laser induced tilt nonlinear process is relevant. We observe that as the intensity is increased the tilt reduces and beyond the intensity, $I_{th} = 8\pi c|\alpha|/\epsilon_a$, the

tilt becomes zero. Thus this geometry leads to saturable type of nonlinearity [10]. The nonlinear function $\mu_{nl}(I)$ in this case is given by:

$$\mu_{nl}(I) = \mu_{\|} - \mu(\theta_\circ) - \frac{\epsilon_a \mu_{\|} |\alpha|}{2\mu_\perp^2 \beta} + \frac{\epsilon_a^2 \mu_{\|}}{16\pi c \mu_\perp^2 \beta} I \tag{7.7}$$

where $\mu(\theta_\circ)$ is the refractive index without the laser field. The corresponding soliton solution is given by:

$$\psi(X) = \sqrt{\frac{2A_2}{B_2}} \frac{1}{\cosh(\sqrt{A_2}X)} \tag{7.8}$$

where $A_2 = 2k_\circ \mu_\perp \nu - \left[\mu_{\|} - \mu(\theta_\circ) - \frac{\epsilon_a \mu_{\|} |\alpha|}{2\mu_\perp^2 \beta}\right]$ and $B_2 = \frac{k_\circ^2 \epsilon_a^2 \mu_{\|}}{8\pi c \beta \mu_\perp}$.

(iii) : In the geometry depicted in figure 7.7 (c), both the laser suppression of c-director fluctuations and the laser induced tilt contribute to intensity dependent changes in the refractive index. This leads to a nonlinear function $\mu_{nl}(I)$ given by:

$$\mu_{nl}(I) = k_B T \sqrt{\frac{\epsilon_a^3}{2\pi^3 K^3}} \sqrt{I/c} + \mu_\perp - \mu(\theta_\circ) + \frac{\epsilon_a \mu_\perp |\alpha|}{2\mu_{\|}^2 \beta} + \frac{\epsilon_a^2 \mu_\perp}{16\pi c \mu_{\|}^2 \beta} I \tag{7.9}$$

Here the first term is due to the process of suppression of c-director fluctuations and the others are contributions from the second process. The soliton solution is like that worked out in section 7.2. It is given by:

$$\psi(X) = \frac{3A_3/B_3}{\left[1 + \sqrt{(\frac{9A_3^2 C}{2B_3^2} + 1)}\ \cosh(\sqrt{A_3}X)\right]} \tag{7.10}$$

where $A_3 = 2k_\circ \mu_\perp \nu + 2k_\circ^2 \mu_\perp \left[\mu_\perp - \mu(\theta_\circ) + \frac{\epsilon_a \mu_\perp |\alpha|}{2\mu_{\|}^2 \beta}\right]$ and $B_3 = 2k_\circ^2 \mu_\perp k_B T \sqrt{\frac{\epsilon_a^3}{2\pi^3 K^3}}$, and $C_3 = \frac{k_\circ^2 \mu_\perp^2 \epsilon_a^2}{8\pi c \mu_{\|}^2 \beta}$. We find that not all values of the parameter ν are allowed. In fact, only those values of ν are allowed which satisfy the inequality:

$$\nu \geq -\frac{2}{9} a_3 - b_3 \tag{7.11}$$

where $a_3 = \frac{(2\epsilon_a \mu_{\|} k_B T)^2 \beta}{\pi^2 \mu_\perp^2 K^3}$ and $b_3 = k_\circ \left[\mu_\perp - \mu(\theta_\circ) + \frac{\epsilon_a \mu_\perp |\alpha|}{2\mu_{\|}^2 \beta}\right]$.

7.3.3 Due to thermal indexing

In addition to the above two processes there can even be the nonlinear process due to laser absorption by the medium which heats up the material with a consequent

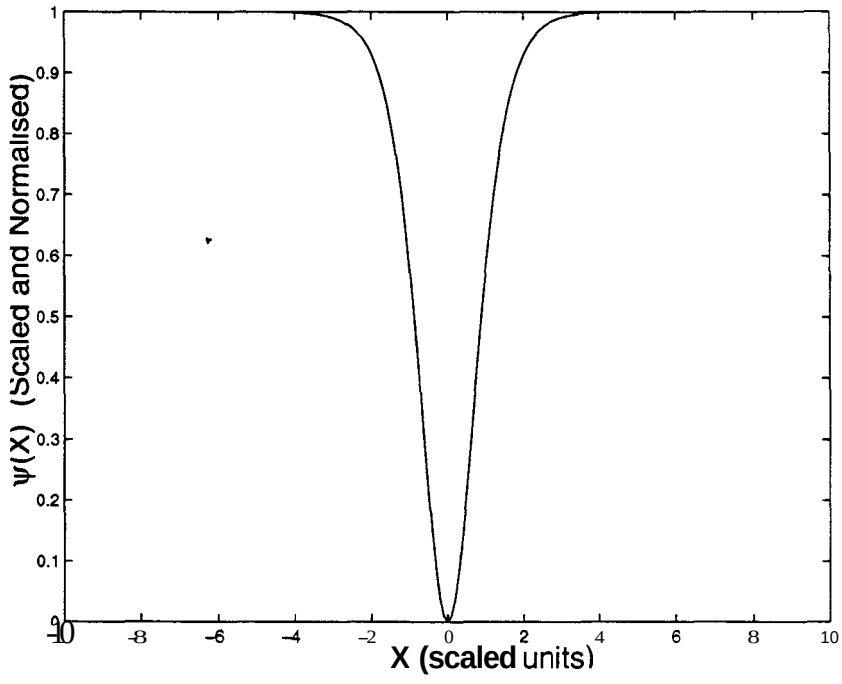

Figure 7.8: *Profile of a typical dark soliton, due to 'thermal indexing' alone.* $X = k_o x$ *is the scaled transverse coordinate and* $\psi(X)$ *is the scaled amplitude of the optical field.*

change in the refractive index. The refractive index change is related to change in temperature as [16]:

$$\delta\mu(I) = \frac{d\mu}{dT}\left(t^2\chi/\pi^2\kappa\right)\ I \ \equiv \eta_2 I \tag{7.12}$$

Here **t** is the sample thickness, χ is the optical absorption coefficient: and κ is the thermal conductivity of the medium. It should be stressed that when thermal indexing is included, we neglect the reduction in the intensity due to absorption. This is justified, as said earlier, when either the sample thickness is very small or absorption is very weak. Bertolotti, et. al., [9] have studied the optical spatial solitons in glass fibres due to thermal indexing by solving the nonlinear Maxwell equation and the thermal diffusion equation. These propagate only for a short distance before instability sets in. But in liquid crystals, due to small sample thickness, low absorption(for optical frequencies) and high nonlinearity, justifying the ***thin – film*** approximation, we can discuss the propagation of stable solitons. Thermal indexing leads to a refractive index change which is either positive or negative. In both the cases the refractive index change is proportional to the laser intensity as in a Kerr media. If the nonlinear

coefficient is positive then we get a bright soliton described by:

$$\mathcal{E}(X,Z) = \left(\frac{2a}{b}\right) \frac{1}{\cosh(\sqrt{a}\,X)} \exp(i\nu Z) \tag{7.13}$$

where $a = 2\mu_\perp k_\circ \nu$ and $b = 2\mu_\perp k_\circ^2 \mu_{nl}(I)$. Here $\mu_{nl}(I) = \frac{d\mu}{dT}\delta T(I)$. If the thermal indexing leads to a negative nonlinear coefficient we get a dark soliton [10] given by:

$$\mathcal{E}(X,Z) = \psi_\circ \left[ia_1 + \sqrt{1-a_1^2}\tanh(X)\right] exp(i\psi_\circ^2 Z) \tag{7.14}$$

Here a_1 is a parameter depending on the nonlinear coefficient, $\psi_\circ^2$ is the intensity of the intense background and the resulting intensity profile is shown in figure 7.8.

7.3.4 Due to thermal indexing and the laser suppression of director fluctuations in nematics

In this case the electric vector of the laser beam is parallel to the director. The thermal nonlinearity here is proportional to $\frac{d\mu_\parallel}{dT}$ and is negative. The corresponding nonlinear Maxwell's equation can be written in terms of $\psi = \mathcal{E}/\mathcal{E}_\circ$ as:

$$i\frac{\partial\psi}{\partial Z} + \frac{\partial^2\psi}{\partial X^2} + |\psi|\psi - \gamma|\psi|^2\psi = 0 \tag{7.15}$$

which is again a nonlinear Schrödinger equation. Here γ is the ratio η_1/η_2 of the two nonlinear coefficients η_1 and η_2 due to the two processes.

The soliton solution for equation (7.15) with the boundary conditions $|\psi(\pm\infty)| \to 0$ is given by:

$$\mathcal{E}(X,Z) = \frac{1}{\left[\frac{1}{3\nu} + exp(-\sqrt{\nu}\,X) - \left(\frac{\gamma}{2\nu} - \frac{1}{(3\nu)^2}\right) exp(\sqrt{\nu}\,X)\right]} exp(i\nu Z) \tag{7.16}$$

The solution here has vanishing asymptotes. Interestingly this equation also permits a kink solution as described in [17]:

$$\psi(X,Z) = \psi_L \left(\frac{1}{1+exp(\delta X)}\right) exp(i\nu Z) \tag{7.17}$$

where,

$$\psi_L = \frac{2}{3\gamma}; \quad \nu = \frac{2}{9\gamma}$$
$$\delta = \pm\sqrt{2/\gamma}/3$$

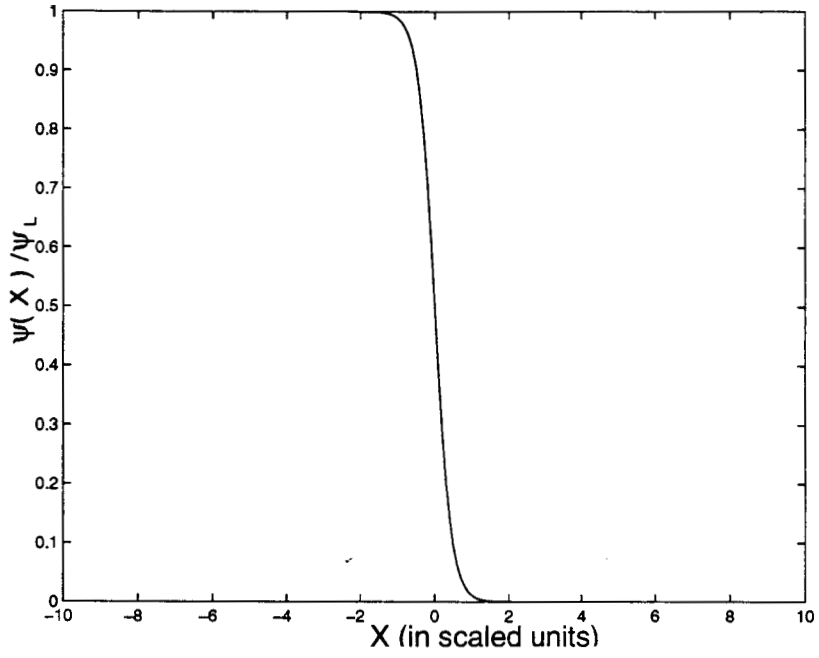

Figure *7.9: A kink soliton when both the nonlinear processes of suppression of director fluctuations and the thermal indexing are operating. The relevant parameters are* $\psi_L = 60.945\ Volt/cm$, $\nu = 20.3cm^{-1}$, $\mu = 4.5cm^{-1}$ *and* $\gamma = 0.01$.

The profile of the kink soliton is shown in the figure 7.9. This is so unlike the earlier soliton profiles. It should be mentioned here that generally kink optical solitons have a phase difference at the two limits i.e., $Z = \pm\infty$ which exist only in the case of *dark solitons*. The present kink soliton by contrast does not possess such a phase difference.

7.3.5 Due to thermal indexing and change of tilt angle in smectics

Here also we consider two cases of light propagation in smectic liquid crystals.

(i) Case I:

We first consider the case where light propagates parallel to the layer normal with the electric vector parallel to the layers of a smectic ***A.*** The system is assumed to be near a smectic ***A*** to smectic C transition.

The nonlinear coefficient for thermal indexing in this geometry is positive. **A** molecular tilt is induced beyond a certain intensity, the threshold for which can be calculated from the free-energy density as discussed earlier. The nonlinear refractive

index $\mu_{nl}(I)$ is given by:

$$\mu_{nl}(I) = \begin{cases} \frac{d\mu_\perp}{dT}\ \frac{d^2\chi}{\pi^2\kappa}\ I & , \quad I < I_{th} \\ \frac{(\mu_\parallel^2-\mu_\perp^2)}{2\mu_\parallel^2\beta}\left(\frac{(\mu_\parallel^2-\mu_\perp)^2 I}{8\pi c} - \alpha\right), & I > I_{th} \end{cases}$$

Initially, when the tilt angle is small, the thermal indexing is proportional to $\frac{d\mu(\theta)}{dT}$ which is positive. As the angle increases $\frac{d\mu}{dT}$ becomes zero and changes sign. Thus beyond a threshold intensity the effective nonlinearity decreases with the intensity. The soliton solution in both regimes are Kerr type. The first solution is given by:

$$\left(\frac{2a_1}{b_1}\right)\ \frac{1}{\cosh(\sqrt{a_1}\ X)} exp(i\nu Z) \tag{7.18}$$

where $a_1 = 2\mu_\perp k_\circ \nu$ and $b = 2\mu_\perp k_\circ^2 \mu_{nl}(I)$ with $\mu_{nl}(I)$ as given above. The second solution is given by:

$$\left(\frac{2a_2}{b_2}\right)\ \frac{1}{\cosh(\sqrt{a_2}\ X)} exp(i\nu Z) \tag{7.19}$$

where $a_2 = 2\mu_\perp k_\circ \nu$ and $b_2 = 2\mu_\perp k_\circ^2 \mu_{nl}(I)$ with $\mu_{nl}(I)$ as given above.

(ii) Case II:

Now we deal with light propagation through a smectic C liquid crystal, along its layers with the electric vector parallel to the layer normal(see figure 7.7 (c)). The nonlinear coefficient due to thermal indexing in this case could be positive or negative depending on the tilt angle 8. Initially it is positive when the angle is large. As the intensity is increased the tilt angle changes and the nonlinear coefficient becomes negative. But the nonlinearity due to change in the tilt angle is always positive. At a certain intensity the tilt angle is zero. Beyond that intensity the second process does not contribute to the nonlinear coefficient. This intensity is given by:

$$I_\circ = \frac{\alpha_\circ(T_{AC} - T)}{\left[\frac{\epsilon_a}{16\pi} + \alpha_\circ\left(\frac{t}{\pi}\right)^2\frac{\chi}{\kappa}\right]} \tag{7.20}$$

At and beyond this intensity the nonlinear coefficient is only due to the thermal indexing and the nonlinearity is proportional to $\frac{d\mu_\parallel}{dT}$ which is negative. The nonlinear refractive index is thus given by:

$$\mu_{nl}(I) = \begin{cases} \mu_\parallel - \mu(\theta_\circ) - \frac{\epsilon_a\mu_\parallel|\alpha|}{2\mu_\perp^2\beta} + \frac{\epsilon_a^2\mu_\parallel}{16\pi c\mu_\perp^2\beta} I + \xi(\theta)\frac{\mu_\perp}{n_{eff}}\frac{d\mu_\perp}{dT}\left(\frac{d}{\pi}\right)^2\frac{\chi}{\kappa} I, & I < I_{th} \\ \frac{d\mu_\parallel}{dT}, & I > I_{th} \end{cases}$$

where, $\mu(\theta_\circ)$ is the refractive index without the laser field. Thus, we get different types of soliton solutions for intensities below and above the threshold even though the nonlinearity is of Kerr-type.

7.4 Critical Power for Spatial Soliton Formation

For the formation of a spatial soliton, optical diffraction must compensate self-convergence. At low intensities in a nonlinear medium with self-focusing nonlinearity, the width of an incident beam decreases continuously and at a certain point the beam width becomes comparable to the laser wavelength. At this stage the optical diffraction becomes important. If the power of the incident beam is high enough the process of self-focusing operates even on the diffracted beam. Hence, the beam continues to converge beyond the diffraction limit destroying the material eventually. Since beam diffraction must compete with self-convergence there exists a threshold intensity. Hence, at a critical power of the laser beam, it is found that the convergence due to nonlinearity can be compensated by the diffraction. At this critical power we get a soliton which also is said to be a self-trapped or self-channeled beam.

In order to calculate the critical power we consider the stability of a plane wave travelling along the z-axis in the nonlinear medium. In this case the Maxwell wave equation becomes:

$$ik_\circ \frac{\partial E}{\partial z} = -1/2 \left(\frac{\partial^2}{\partial x^2} + \frac{\partial}{\partial y^2} \right) E - \mu_{nl}(I) E \qquad (7.21)$$

which is a generalised Schrodinger equation. To find the stability of an infinite plane wave we consider the spatial evolution of perturbations along the direction of propagation [18]. The dispersion relation with the nonlinearity gives for the wavevector:

$$k^2 = \frac{\omega^2 \epsilon(\omega)}{c^2} + 2\mu_{nl}(\mathrm{I})$$

$$k = k_\circ + \mu_{nl}(I)/k_\circ$$

where $k_\circ = \omega\sqrt{\epsilon(\omega)}/c$, and $\mu_{nl}(I)$ is the nonlinear refractive index. Hence, the

amplitude of the unperturbed beam is of the form $E_o(z) = E, exp[i\ \mu_{nl}(I)\ z/k_o]$ where E_o is the amplitude of the incident laser beam. We write the perturbation in E in the form:

$$\delta E(r) = [A\, exp(i(q \cdot r + k_z z)) + \mathcal{B}^*\, exp(-i(\mathbf{q} \cdot r + k_z z))]\, exp(i\mu_{nl}(I) z/k_o) \quad (7.22)$$

Here q is a vector in the x – y plane. Substituting this in the equation (7.21) and collecting the groups of terms in $exp(\pm i(q \cdot r + k_z z))$, we get:

$$\left(\frac{q^2}{2} - \mu_{nl}(I) + k_o k_z\right) \mathcal{A} - \mu_{nl}(I)\mathcal{B} = 0$$

$$-\mu_{nl}(I)\mathcal{A} + \left(\frac{q^2}{2} - \mu_{nl}(I) - k_o k_z\right) \mathcal{B} = 0$$

The condition that a nontrivial solution for these equations exist is that the determinant of the coefficients must vanish. This condition gives:
$k, = \pm \frac{q}{2k_o} \sqrt{q^2 - 4\mu_{nl}(I)}$. When μ_{nl} is positive, i.e., in a focusing media, if

$$q^2 \leq 4\mu_{nl}(I) \quad (7.23)$$

then k, becomes imaginary. This gives an exponentially increasing term in the perturbation and the wave becomes unstable.

In a beam of radius R, the wavevector of perturbation transverse to propagation direction is restricted by $q \geq 1/R$. This sets the upper limit on the q values which is responsible for the focusing instability. Thus the equation (7.23) gives the critical value of the intensity (and thus the electric field). If the nonlinearity is of Kerr type then $\mu_{nl} = \eta I = \eta E_o^2$ giving $E_o^2 \approx 1/\eta R^2$. As the power in a laser beam is equal to $E_o^2 R^2$, the critical power is then given by $P_{cr} \approx 1/77$. It is thus independent of the beam width.

We now study the same problem in the presence of only the suppression of director fluctuations i.e., $\mu_{nl} = \eta_1 \sqrt{I} = \eta_1 E_o$. The inequality (7.23) becomes $q^2 < 4\eta_1 \sqrt{I}$. The expression for the critical power hence is:.

$$P_{cr} \approx 1/\left(\eta_1^2 R^2\right) \quad (7.24)$$

Hence the critical power decreases as the beam size increases.

We next consider the simultaneous presence of suppression of the director fluctuations and the thermal indexing. In this case the condition (7.23) yields for the critical field E_o

$$\left(\eta_1 E_o - \eta_2 E_o^2\right) R^2 \approx 1 \qquad (7.25)$$

This leads to two critical powers given by:

$$P'_{cr} \approx \left[\frac{\eta_1 R_o - \sqrt{\eta_1 R_o^2 - 4|\eta_2|}}{\eta_2}\right]^2$$
$$P''_{cr} \approx \left[\frac{\eta_1 R_o + \sqrt{\eta_1 R_o^2 - 4|\eta_2|}}{\eta_2}\right]^2$$

We notice that the critical power exists only if the nonlinear coefficients satisfy the inequality:

$$\eta_1 R_o^2 > 4|\eta_2| \qquad (7.26)$$

Thus we see that irrespective of the strengths of the nonlinear coefficients, a width R for the beam can always be so chosen that the inequality (7.26) is satisfied. The first(lower) critical power P'_{cr}, occurs when the effect of beam diffraction exactly balances the effects of suppression of director fluctuations. At this power the thermal indexing does not contribute significantly. The second(higher) critical power P''_{cr}, occurs when the effect of beam diffraction balances the defocusing effects due to thermal indexing and by the focusing effect of suppression of director fluctuations. Thus existence of two nonlinear processes leads to new results in the critical power required for soliton formation.

Bibliography

[1] Yu. S. Kivshar, Opt. & Quant. Elec., **30,** 571, (1998)

[2] L. Lam, Chaos, Solitons and Fractals, **5(10)**, 2134 (1995)

[3] Hasegawa and Kodama, Proc *IEEE,* 69, 1145 (1981)

[4] L. Lam and Y. S. Yung, in *Modern Topics in Liquid Crystals, From Neutron Scattering to Ferroelectricity*(Ed. A. Buka), (World Scientific, Singapore), 187 (1992)

[5] J. A. Reyes and Palffy-Muhorray, Phy. Rev., **E58(5)**, 5855 (1998)

[6] Rodriguez and Reyes, Jl. Mol. Liq., 71, 115 (1997)

[7] M. Warenghem et. al., Jl. Non. Opt. Phy. & Mat., **8(3)**, 341 (1999)

[8] I. C. Khoo, *Liquid Crystals, Physical Properties and Nonlinear Optical Phenomena* (John Wiley and sons, Newyork) 1995

[9] M. Bertolotti, R. Li. Voti, S. Marchetti, and C. Sibilia, Opt. Commun., 133, 578 (1997)

[10] N. N. Akhmediev and A. Ankiewicz, *Solitons - Nonlinear Pulses and Beams* (Chapmann and Hall, London) 1997

[11] A. Yariv and P. Yeh *Optical Waves* in *Crystals, Propagation and Control of Laser Radiation* (John-Wiley and Sons, Inc., Newyork); 1984

[12] S. A. Pikin, *Structural Transformations in Liquid Crystals* (Gordon and Breach Science Publishers, Newyork), 1991

[13] S. K. Srivatsa and G. S. Ranganath, Opt. Commun., **180(4-6)**, 343 (2000)

[14] N. V. Tabiryan, **A.** V. Sukhov and B. Ya. Zel'd ovich, Mol. Cryst. Liq. Cryst., 136, 1 (1986)

[15] I. C. Khoo, Jl. Non. Opt. Phy. & Mat., **8(3)**, 305 (1999)

[16] Simoni. F, *Nonlinear Optical Properties of Liquid Crystals and Polymer Dispersed Liquid Crystals.,* (World Scientific, Singapore) 1997

[17] K. Hayata and M. Koshiba, Optical Review, **2(1)**, 4 (1995)

[18] L. Landau and Lifshitz, *Electrodynamics of Continuous Media* (Second Revised Edition, Pergamon Press, Oxford) 1984